Horizon 2020 Programme

METIS

Research and Innovation Action (RIA)

This project has received funding from the European Union's Horizon 2020 research and innovation programme under grant agreement No 945121

Start date : 2020-09-01 Duration : 57 Months

Report on damage/failure relevant ground motion intensity measures

Authors : Dr. Matjaz DOLSEK (UL), Matja? Dolsek (UL), Neja Fazarinc (UL), Paolo Bazzuro (IUSS), Nevena Sipcic (IUSS), Pablo Alfonso Garcia (IUSS), Georgios Triantafyllou (IUSS , EDF), Irmela Zentner (EDF), Angeliki Gerontati (NTUA), Dimitrios Vamvatsikos (NTUA)

METIS - Contract Number: 945121

Project officer: Katerina PTACKOVA

Document title	Report on damage/failure relevant ground motion intensity measures
Author(s)	Dr. Matjaz DOLSEK, Matja? Dolsek (UL), Neja Fazarinc (UL), Paolo Bazzuro (IUSS), Nevena Sipcic (IUSS), Pablo Alfonso Garcia (IUSS), Georgios Triantafyllou (IUSS , EDF), Irmela Zentner (EDF), Angeliki Gerontati (NTUA), Dimitrios Vamvatsikos (NTUA)
Number of pages	62
Document type	Deliverable
Work Package	WP6
Document number	D6.3
Issued by	UL
Date of completion	2024-09-23 08:16:32
Dissemination level	Public

Summary

This report offers a detailed examination of ground motion IMs pertinent to the assessment of damage and failure in structural engineering, with a specific focus on their application within nuclear power plant safety evaluation. Various scalar IMs are examined through a series of case studies and evaluations to better understand their efficacy in predicting structural response and fragility under seismic loading conditions. The document begins with an overview of damage and failure-relevant IMs, providing both background context and an exploration of scalar and vector-valued measures. Seismic fragility assessment of SSCs can be approached through various methodologies. As discussed in Section 1, numerous scalar and vector IMs are available for this analysis. However, the seismic fragility and risk analysis are not only affected by the choice of IMs but are also dependent on the ground motions used to assess the structure's response and the seismic analysis type. Consequently, the ground motion selection process is often constrained by Multiple Stripe Analysis and Incremental Dynamic Analysis, which are commonly employed seismic analysis methods, also used in the case studies presented in this report. The first case study explores the optimization of GMM-relevant scalar IMs (PGA, Sa and AvgSa) for the AP1000 reactor model through the analysis of generic ground motions. Through a simplified soil-structure interaction analysis, it examines various components such as the reactor building and service water pump. The second case study investigates the impact of hazard consistency on IM optimality assessment, considering different hazard scenarios influencing the selection and effectiveness of IMs. Lastly, the third case study evaluates record selection schemes, IMs, and fragility analysis methods based on the METIS case study. It provides insights into ground motion characteristics, reactor building modeling, fragility analysis approaches, and summarizes the key findings and implications derived from the study. The conclusions drawn from the analysis of various IMs, such as PGA, Sa and AvgSa, in this study emphasize the complexity and importance of selecting appropriate measures for seismic fragility assessment, particularly in the context of NPPs and summarize the main findings from the three case studies.

Approval

Date	By
2024-09-23 10:54:16	Mrs. Shadi FATHABADI (TUK)
2024-09-23 11:03:23	Dr. Irmela ZENTNER (EDF)

METIS

Seismic Risk Assessment for Nuclear Safety

Research & Innovation Action

NFRP-2019-2020

Damage/failure relevant ground motion intensity measures, record selection/generation and site response analysis schemes

Deliverable D6.3

Version N°4

Authors:

Matjaž Dolšek, Neja Fazarinc (UL)

Paolo Bazzuro, Nevena Sipcic, Pablo Alfonso Garcia (IUSS)

Georgios Triantafyllou (IUSS , EDF), Irmela Zentner (EDF)

Angeliki Gerontati, Dimitrios Vamvatsikos (NTUA)

This project has received funding from the Horizon 2020 programme under grant agreement n°945121. The content of this presentation reflects only the author's view. The European Commission is not responsible for any use that may be made of the information it contains.

Document Information

Grant agreement	945121
Project title	Methods And Tools Innovations For Seismic Risk Assessment
Project acronym	METIS
Project coordinator	Dr. Irmela Zentner, EDF
Project duration	1st September 2020 – 31st May 2024 (57 months)
Related work package	WP6 – Beyond Design and Fragility Analysis
Related task(s)	Task 6.3 Determination of damage/failure relevant ground motion intensity measures and record selection
Lead organisation	UL
Contributing partner(s)	IUSS, EDF, NTUA, UL
Due date	29.2.2024
Submission date	20.9.2024
Dissemination level	Public

History

Date	Version	Submitted by	Reviewed by	Comments
29.2.2024	N°1	Matjaž Dolšek		Submitted to Project Leader
7.5.2024	N°2	Anže Babič	Reviewer	Added directly into text, mainly editorial issues.
15.5.2024	N°3	Matjaž Dolšek		Submitted to Project Leader
20.9.2024	N°4	Matjaž Dolšek		Uploaded

Table of Contents

List of figures

List of tables

Abbreviations and Acronyms

Acronym	Description
ASB	Coupled Auxiliary and Shield Building
CCDF	Conditional (cumulative) probability distribution function
CIS	Containment Internal Structure
COV	Coefficient of variation
CS	Conditional spectrum
ECDF	Empirical Cumulative Density Function
EDP	Engineering demand parameter
EPRI	Electrical Power Research Institute
FE	Finite elements
FSA	Floor spectral acceleration
GMM	Ground motion model
GM	Ground motion
GMPE	Ground motion prediction equation
GMR	Ground motion record
HCLPF	High Confidence of Low Probability of Failure
IDA	Incremental Dynamic Analysis
IM	Ground motion intensity measure
IML	Ground motion intensity measure level
MAF	Mean Annual Frequency
MSA	Multiple Stripe Analysis
NPP	Nuclear Power Plant
nSDOF	Nonlinear single degree of freedom system
PBEE	Performance-Based Earthquake Engineering
PFA	Peak floor acceleration
PGA	Peak ground acceleration
PGD	Peak ground displacement
PGV	Peak ground velocity
PoE	Probability of Exceedance
PSDA	Probabilistic Seismic Demand Analysis

PSHA	Probabilistic Seismic Hazard Analysis
PWR	Pressurized water reactor
RSM	Relative Sufficiency Measure
SCV	Steel Containment Vessel
SPRA	Seismic Probabilistic Risk Assessment
SSI	Soil-structure Interaction
SSC	Structures, systems and components
TF	Transfer Function
UHS	Uniform Hazard Spectrum
WP	Work Package

Introduction

Investigating the impact of types of intensity measures (IMs) in seismic design and risk assessment of nuclear power plants is important because IMs affect the process and the results of design and seismic risk assessment. While PGA is commonly utilized, particularly for stiff structures, systems, and components (SSC) where seismic force correlates well with PGA, PGV may be more suitable for SSCs with intermediate frequencies, and PGD may be suitable for flexible SSCs. However, advanced measures have also been introduced to address the variability in IMs and enhance their effectiveness. As the efficiency and sufficiency of IMs vary depending on structural characteristics and seismic conditions, comprehensive studies evaluating different IMs' performance are essential for informed decision-making in structural engineering and risk assessment contexts.

This report offers a detailed examination of ground motion IMs pertinent to the assessment of damage and failure in structural engineering, with a specific focus on their application within nuclear power plant safety evaluation. Various scalar IMs are examined through a series of case studies and evaluations to better understand their efficacy in predicting structural response and fragility under seismic loading conditions.

The document begins with an overview of damage and failure-relevant IMs, providing both background context and an exploration of scalar and vector-valued measures. Seismic fragility assessment of SSCs can be approached through various methodologies. As discussed in Section 1, numerous scalar and vector IMs are available for this analysis. However, the seismic fragility and risk analysis are not only affected by the choice of IMs but are also dependent on the ground motions used to assess the structure's response and the seismic analysis type. Consequently, the ground motion selection process is often constrained by Multiple Stripe Analysis and Incremental Dynamic Analysis, which are commonly employed seismic analysis methods, also used in the case studies presented in this report.

The first case study explores the optimization of GMM-relevant scalar IMs (PGA, Sa and AvgSa) for the AP1000 reactor model through the analysis of generic ground motions. Through a simplified soil-structure interaction analysis, it examines various components such as the reactor building and service water pump.

The second case study investigates the impact of hazard consistency on IM optimality assessment, considering different hazard scenarios influencing the selection and effectiveness of IMs.

Lastly, the third case study evaluates record selection schemes, IMs, and fragility analysis methods based on the METIS case study. It provides insights into ground motion characteristics, reactor building modeling, fragility analysis approaches, and summarizes the key findings and implications derived from the study.

The conclusions drawn from the analysis of various IMs, such as PGA, Sa and AvgSa, in this study emphasize the complexity and importance of selecting appropriate measures for seismic fragility assessment, particularly in the context of NPPs and summarize the main findings from the three case studies.

1. Overview of Damage/failure relevant ground motion intensity measures

Traditional seismic design and analysis for civil structures and nuclear power plants (NPPs) have relied on the utilisation of peak ground acceleration (*PGA*) and spectral acceleration (S_a) as primary earthquake IMs. However, numerous studies have delved into the effectiveness and adequacy of these IMs and sought to identify more robust and suitable alternatives. Still, the impact of performing PSHA in connection with IMs was usually not considered in assessments of the optimal choice of IM. This section aims to provide a comprehensive exploration of these IMs, encompassing both scalar and vector types, along with their distinctive attributes.

Firstly, an initial discussion on the use of scalar and vector-valued IMs within the seismic loss and fragility assessment framework is presented. Section 1.1 concludes with the categorisation of IMs into scalar and vector-valued IMs. Section 1.2 delves into a thorough literature review of scalar IMs, encompassing both non-structure-specific and structure-specific IMs. Finally, section 1.3 provides a concise overview of vector-valued IMs.

1.1. Background

In the past, the seismic design of structures, systems and components (SSCs) was mostly based on the scenario-based seismic performance assessment, considering one or more "design earthquakes", typically defined by source, magnitude, and distance, where the ground motions were estimated deterministically. The first steps towards probabilistic approaches in seismic design were made in the late 1970s with the publication of the ATC-3-06 report (ATC, 1978). The report proposed performance evaluation based on the relationship between estimated and allowable inter-storey drifts and thus introduced the use of deformation-based response and capacity measures as metrics of performance.

In the following two decades, studies were made to develop more refined performance objectives, such as acceptable risk of experiencing different levels of damage or loss (e.g. Vision 2000 report, SEAOC, 1995). Levels of damage were further linked to ground motions with certain return periods, which were expressed deterministically and conservatively. The basic framework that is the state-of-the-art used for current studies was developed by The Pacific Earthquake Engineering Research Center (PEER) in 2000. The proposed Performance-Based Earthquake Engineering (PBEE) framework (Cornell and Krawlinker, 2000; Moehle and Deirlein, 2004) proposed the idea that the seismic risk can be expressed in terms of mean annual frequency (MAF) of exceeding a limit state, where the randomness regarding the ground motion intensity depends also on an IM. The IMs can be scalar parameters or vectors composed of a few different scalar parameters. IMs serve as intermediate variables between ground motion hazard and structural demand and enable the complete prediction of performance through the response model, damage model, and loss model (Figure 1) without the demanding probabilistic description of the ground-motion time history by means of a stochastic model.

In parallel, the seismic risk assessment of NPPs was developed with several different approaches for the fragility analysis, which is one of the essential steps in the Seismic Probabilistic Risk Assessment (SPRA) methodology (EPRI, 2003). The aim of the fragility analysis is to design fragility curves, which can be developed with different levels of detail, different modelling assumptions and restrictions and considered failure modes, as discussed by Zentner et al. (2017). A common approach is the Safety-Factor method established in the 1970s and further refined by Kennedy et al. (1980) and Kennedy and Ravindra (1984), where a product of safety factors is used to account for the assessed uncertainties and seismic margins. The advantage of this method is that it doesn't require time-consuming numerical simulations to provide the median capacity and the standard deviation that determine the fragility curve. The drawback of the methodology is that the structural capacity and demand defined with the product of seismic margins assumes linear relations between the parameters and independence between the variables that affect the seismic demand and capacity.

Alternatively, numerical simulations can be used to evaluate the fragility of the structure, where the ground motions have to be consistent with the site-specific characteristics and site-specific seismic hazard. A lognormal cumulative distribution function is usually used to define the fragility curve, which reduces computational effort. An overview of the possible methodologies for fragility estimation based on numerical simulations is available in Porter et al. (2007). The number of analyses needed for satisfactory accuracy of the curves determined with the least-square approach and maximum likelihood method can be estimated based on the findings by Gehl et al. (2015).

Sometimes family of fragility curves is used to account for the uncertainties. Those uncertainties are mainly epistemic because of the incomplete knowledge about the parameters and the related distributions needed for the fragility assessment and were a subject of several studies (e. g. see Liel et al., 2009; Ellingwood and Kinali 2009).

Recently, more refined approaches have been developed for the definition of the fragility curves, for example, non-parametric fragility functions with Gaussian kernel smoothing (Noh et al., 2015), generalized linear and additive models (Rossetto et al., 2015) and fragility curves based on multivariate probability distributions (Zentner, 2016).

For the SPRA analysis, common approaches for the estimation of the fragility curves are the maximum likelihood method and linear regression in log-space, which don't require spectral matching or ground motion scaling. The first one is more appropriate for binary damage measures, while the latter requires continuous failure measures. While IDA results could be considered for estimating the parameters of the fragility curves using both statistical approaches, the IDA-based fragility curves are more commonly assessed for ordinary buildings than for NPP structures. The selection of an appropriate IM is crucial in the SPRA analysis, where the development of the fragility curves is usually based on a single scalar IM, rather than a vector-valued one, which could better constrain the structural response. Thus, it is important that the scalar IM meets the criteria regarding efficiency and sufficiency, further presented in the following paragraphs.

Regardless of the observed type of structure and the adopted framework, namely PBEE or SPRA, the main steps of the analysis are analogous, as presented in Figure 1 with a key point being the evaluation of the fragility curves which express the probability of the structure as a function of an IM (Sainct et al., 2020).

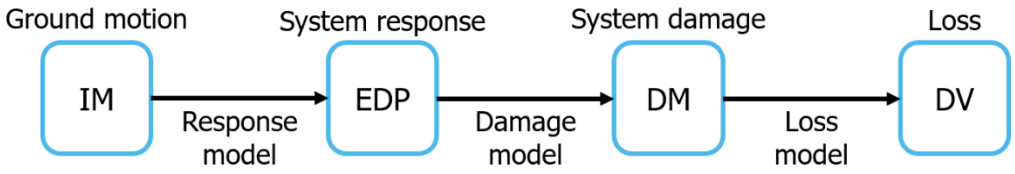

Figure 1: Schematic illustration of prediction of PBEE or SPRA framework.

The structural demand estimates, which serve for further damage and loss prediction, and the ground motion hazard are thus linked with the equation for mean annual frequency of exceeding a given Engineering Demand Parameter (EDP), which can be numerically evaluated as follows:

$$\lambda_{EDP}(y) = \sum_{all\ x_i} P(EDP > y|IM = x_i) \cdot \Delta\lambda_{IM}(x_i), \quad (1a)$$

where $\lambda_{EDP}(y)$ represents the annual frequency of exceeding a given EDP value y, $\lambda_{IM}(x_i)$ the annual frequency of exceeding a given IM value x_i and $P(EDP > y|IM = x_i)$ the probability of exceeding a certain EDP level, given $IM = x_i$. Note that Eq. (1a) needs to be generalised if the IM is a vector, rather than a scalar (e.g. Baker,2007; Alembagheri, 2018).

The risk equation for the estimation of the mean annual rate of failure can also be expressed as (e.g. Jalayer et al., 2017):

$$\lambda_{LS}(y) = \int_0^\infty P(Y > 1|IM) \cdot d\lambda_{IM}(IM), \quad (1b)$$

where $P(Y > 1|IM)$ is the probability of failure at given level of IM, i. e. the fragility curve and $d\lambda_{IM}(IM)$

the defined hazard curve for the observed IM. Since the accuracy of damage and loss estimation highly affects the probabilistic risk assessment based on Eq. (1b), a selection of suitable IM that accounts for the ground motion randomness is crucial to obtain a strong correlation between the adopted IM and the predicted EDP.

The estimation of EDP from IM may be approached by different methods that are discussed in detail elsewhere (e.g. Jalayer, 2003; Baker, 2007). If the adopted IM is a scalar, the most common approaches for EDP estimation are:

- incremental dynamic analysis (Vamvatsikos and Cornell, 2002),
- cloud method that includes the regression analysis on response data from unscaled ground motions, commonly used to further estimate the efficiency of the IM (e.g. Jalayer, 2003),
- stripe analysis considering scaled records to the target IM level and fit a parametric distribution to response results (e.g. Jalayer 2003).

For vector IMs ($\boldsymbol{IM} = \{IM_1, IM_2,\ldots\}$) similar approaches were developed, where it is usually assumed that one of the parameters (IM_1) serves as a dominant predictor of the structural response and is therefore treated differently than others that serve as supplementary predictors ($IM_2, IM_3,\ldots$) (Baker, 2007). The developed approaches for estimating EDP for a vector of IMs as discussed by Baker (2007) are:

- cloud analysis with a multiple linear regression,
- to scale records to the target IM_1 and regress on additional parameters,
- to fit a conditional distribution for IM_1 capacity to IDA results.Only the IM_1 is scaled during IDA, until the EDP value of interest is obtained. The $IM_1 - EDP$ curves are then plotted against IM_2 to the level of EDP of interest. The set of points, where these curves cross the EDP value of interest define a set of IM capacity values. Linear regression is then used to find the conditional mean od IM_1, given IM_2, taking into account that the IMs are correlated.
- to scale records to specified IM_1 levels and calculate empirical CCDF distributions,
- to process records to match target values of all $\boldsymbol{IM}$ parameters.

Vector IMs allow improved estimation of EDP distributions but are complicated to use, usually requiring complex analysis procedures (more simulations of structural response, significant number of records, etc.). Thus, methods that achieve the gains of vector IMs while simplifying the process of analysis were developed, for example:

- to fit a distribution to a stripe of data after re-weighting to match a target distribution of $IM_2|IM_1$ (Jalayer, 2003; Shome and Cornell, 1999), which involves scaling a set of ground motions to IM_1, discretising the IM_2 into a set of bins and re-weighing the data set (each of the records) to have the proper distribution of $IM_2|IM_1$ (obtained from vector-valued PSHA or disaggregation if $IM_2 = \varepsilon$). The weighted record set has a probability distribution equal to the target thus the scalar stripe methods can be applied,
- to scale records to a specified level of IM_1, selecting the records to match the desired distribution of secondary parameters.

The proposed hybrid methods achieve the gains of vector IM methods but require simpler processing than with the explicit vector procedures. The pros of the first hybrid method are that the records do not need to be re-selected at each IM_1 level, while the cons are that for some records, the weights of the results will be zero or nearly zero, essentially throwing away data, with the curse of dimensionality also

representing a problem when many IMs are employed. The second hybrid model only requires the scalar-IM processing procedure, but the records need to be selected more carefully and likely re-selected for different IM_1 levels (Baker 2007).

As previously outlined, the IMs can be classified as scalars or vectors (Figure 2). Some scalar IMs can be non-structure specific (i.e. determined directly from the ground-motion time histories). Such IMs are acceleration-related, velocity-related, and displacement-related IMs. Other scalar IMs are structure-specific, often related to the vibration period of the structure (spectral), the period range (integral), or multiple periods (multi-parameter), as categorised by Mollaioli et al. (2013) and Ebrahimian et al. (2015). The overview of the literature, related to scalar and vector IMs is given in Section 1.1. and Section 1.2.

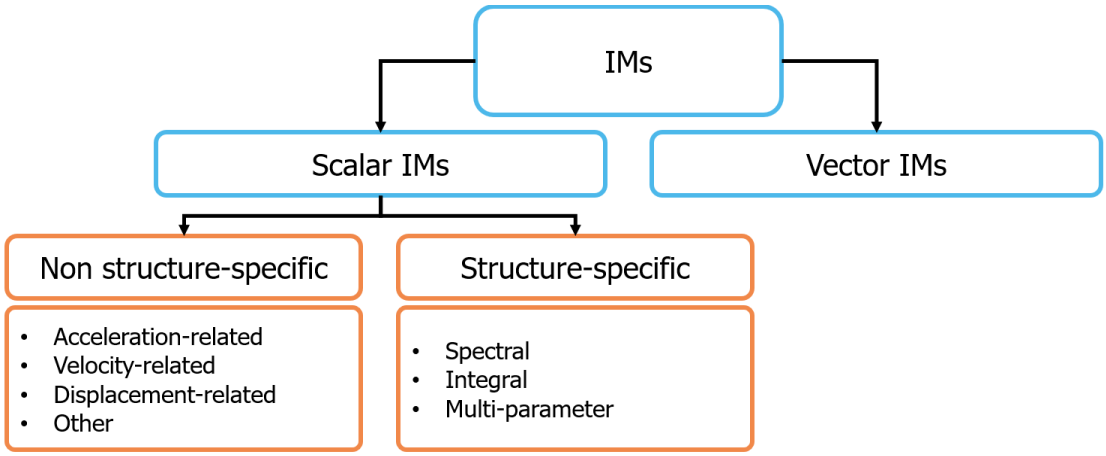

Figure 2: IM categorisation with an emphasis on scalar IMs.

As evident from the tables in Sections 1.1 and 1.2, there exists a wide array of different IMs, with ongoing developments and research in this area. The careful selection of an appropriate IM plays a pivotal role in optimising the seismic analysis and seismic hazard assessment process. Therefore, multiple scholars have formulated specific criteria for assessing the suitability of proposed IMs.

The chosen IM should effectively capture the ground motion's characteristics and align with the requirements of a Probabilistic Seismic Hazard Analysis (PSHA), considering the prevailing framework conditions. To facilitate an objective comparison among various IMs and aid in selecting an optimal IM, several characteristics can be examined, such as efficiency, sufficiency, practicality, proficiency, scalability, complexity, transparency, hazard computability, etc.

The concept of IM efficiency as used today was initially introduced by Luco and Cornell (Luco & Cornell, 2007) in 2007. Efficiency, in this context, quantifies the extent of dispersion observed within an EDP when linked to a specific IM , thus being one of the most important features in the assessment of the seismic vulnerability of structures. It is usually evaluated through the conditional standard deviation $\beta_{EDP|IM}$ obtained from linear regression. Employing an efficient IM has the potential to substantially reduce the number of necessary nonlinear dynamic analyses and earthquake simulations required for vulnerability assessment (e.g. Baker & Cornell, 2004). In mathematical terms, high efficiency enables a more precise and simple determination of the conditional probability distribution of EDP. However, it should be noted that an IM can never be completely efficient, otherwise, it would correspond to the EDP. Consequently, every IM exhibits some degree of inefficiency.

Another important property that an IM should have is sufficiency. It can be used to assess the conditional dependence of an EDP at a given IM and various seismic parameters such as magnitude, distance, and other important fault characteristics, including the ε parameter. A perfectly sufficient IM allows the prediction of structural response independently of earthquake magnitude, source-to-site distance and other earthquake characteristics. Moreover, it enables the selection of arbitrary earthquake time histories for structural analysis without the additional consideration of seismic attributes and potential earthquake effects, such as velocity pulses (Luco & Cornell, 2007; Marafi et al., 2016).

The above condition can be expressed mathematically as follows:

$$P\left[EDP > x \middle| IM, M_w, R_{rup}, other\right] = P[EDP > x|IM], \quad (2)$$

where M_w is the magnitude of the considered ground motion, R_{rup} the considered site-to-source distance and $other$ are other parameters charactersing fault mechanisms, site and path effects.

If this condition is satisfied, the basic equation of PSDA (e.g. (Bojorquez et al., 2008)):

$$\lambda_{EDP}(x) = \sum_i v_i \int_{IM} \int_{M} \int_{R} P[EDP > x|IM, M, R] f(IM|M, R) f(M, R)\, dr\, dm\, d(im) \quad (3)$$

can be simplified as follows (Bojórquez & Iervolino, 2011):

$$\lambda_{EDP}(x) = \int_{IM} P[EDP > x|IM] |d\lambda_{IM}(im)|, \quad (4)$$

where $\lambda_{EDP}(x)$ is the mean annual exceedance probability of the EDP of a value x and $d\lambda_{IM}(im)$ the differential of the hazard curve of the IM.

Sufficiency can be determined similarly to efficiency using a regression analysis where it is quantified by the *p*-value, i.e. the probability of rejecting the null hypothesis, which proves the independence of IM from the remaining seismic hazard characteristic. Thus, a higher *p*-value indicates a sufficient IM and none or only a small dependence is observed with respect to the EDP (Buratti, 2012).

An alternative to determining the sufficiency of IMs is the relative sufficiency measure (RSM), which was introduced in 2012 by Jalayer et al. (2012), who defined an IM as perfectly sufficient if the following criteria are met:

$$P\left[EDP|\boldsymbol{a_g}\right] = P\left[EDP|IM(\boldsymbol{a_g})\right] \quad (5)$$

where $P\left[EDP|\boldsymbol{a_g}\right]$ is the probability of the structural response reaching a certain level of EDP during the observed ground motion and $\boldsymbol{a_g}$ represents the acceleration time history. The above equation indicates that the selected IM would provide as much information about the EDP as the entire ground motion time history which further means that with negligible modelling uncertainty, a perfectly sufficient IM would fully determine the EDP.

The sufficiency of an IM can be evaluated through the concept of relative entropy $D[\cdot]$, which measures the relative difference in the information about the EDP if knowing the entire ground motion history, compared to only knowing the IM, mathematically formulated as:

$$D\left[EDP|IM|\boldsymbol{a_g}\right] = \int P\left[EDP|IM(\boldsymbol{a_g}), \boldsymbol{a_g}\right] \log_2 \frac{P\left[EDP|IM(\boldsymbol{a_g}), \boldsymbol{a_g}\right]}{P\left[EDP|IM(\boldsymbol{a_g})\right]} dEDP \quad (6)$$

Since the aim is usually to compare the sufficiency of several IMs, Jayaler et al. (2012) used the above equation to formulate the so-called relative sufficiency measure (RSM), which measures the gain of information about the uncertain structural response parameter if knowing IM_2 instead of IM_1. RSM, denoted as I, thus represents the expected value $E(\cdot)$ of the difference of relative entropies $D(\cdot)$ of IM_1 and IM_2:

$$\begin{aligned} I(EDP|IM_2|IM_1) &= E\left[D\left(EDP|IM_1|\boldsymbol{a_g}\right) - D\left(\mathrm{EDP}\middle|IM_2|\boldsymbol{a_g}\right)\right] \\ &= \int \log_2 \frac{P\left[EDP(\boldsymbol{a_g})|IM_2(\boldsymbol{a_g})\right]}{P\left[EDP(\boldsymbol{a_g})|IM_1(\boldsymbol{a_g})\right]} P(\boldsymbol{a_g}) d\boldsymbol{a_g} \end{aligned} \quad (7)$$

The logarithm calculated in base two implies that the RSM is expressed in terms of bits of information. If RSM takes a positive value it means that IM_2 is more sufficient than IM_1 and vice versa. If the value of RSM equals two zero, the observed IMs can be considered equally sufficient.

Efficiency and sufficiency are thus two of the most important characteristics that an IM should exhibit and are the focus of current studies investigating existing and new scalar and vector IMs. The estimation is achieved through Probabilistic Seismic Demand Analysis (PSDA). Within this framework, Baker (2007) has compiled and compared several methodologies applicable to both scalar and vector IMs, which contribute significantly to assessing IM efficiency.

The practicality of the considered IMs can be measured by one of the regression parameters when defining the PSDA with linear regression and it shows the correlation between the IM and the EDP. If there is little or no dependence of the level of EDP upon the level of IM, the IM is considered not practical (Padgett et al., 2008). Padgett et al. (2008) also proposed proficiency as a composite measure of efficiency and practicality, which assists in the selection of the optimal IM by reducing the challenge of balancing different factors and optimality measures.

The scalability or scaling robustness refers to the feature that EDP remains unbiased when scaling the ground motion to a given value of IM compared to the EDP obtained from unscaled ground motion. This characteristic of the IM implies that the structural response will have a low dependence on the scaling factor and it is measured with the *p*-value of the regression analysis between the residuals and the used scaling factors in IDA analysis (Heshmati and Jahangiri, 2021).

An IM is considered transparent if it clearly quantifies the individual contributions of spectral acceleration, shape and the duration of the ground motion, which are the parameters needed for the comparison and selection of the appropriate ground motions (Marafi et al., 2016).

In addition to the characteristics of IMs already mentioned, complexity and related hazard computability must also be considered. Especially in view of the PSHA, it is important that the IM used can be easily calculated or inferred from the time histories since PSHA represents a large computational effort that is increased with a complex IM (Giovenale et al., 2004). Currently, the hazard curves are available mostly for PGA and $S_a(T)$ (Hariri-Ardebili and Saouma, 2016). With IMs that require, for example, pushover analyses or other complicated and computationally intensive steps to calculate, the time and computational effort required can easily increase strongly (Baker & Cornell, 2008a).

Besides the numerous IMs that can be used, several different EDPs can also be considered, since the structural damage is not only reflected by the maximum deformations (displacement-based parameters) or forces (force-based parameters) but also by the maximum accelerations and amount of dissipated energy due to cyclic loading (energy-based demand parameters). Some more commonly studied EDPs are maximum roof drift ratio, maximum inter-storey drift ratio, and maximum floor acceleration.

From the literature review, it can be concluded, that the development of the appropriate framework, regarding the selection of the suitable IM, analysis approach, and suitable EDP should be considered highly case-specific. This conclusion is based on the observations of different authors who realised that there are differences in the efficiency and sufficiency of the examined IMs when used on different types of structures. For example, some IMs proved to be more suitable for structures with longer vibration periods, while others performed better for structures with shorter vibration periods. Some IMs better accounted for the non-linearity of the response than others. Furthermore, it was observed that different IMs were suitable for different types of ground motions (e.g. near-fault, pulse-like, etc.). Furthermore, it should be considered that even the most efficient and sufficient IMs may not be the most suitable to use if an appropriate hazard definition framework doesn't exist to support their implementation, thus the development and future studies should focus on that interconnection. The overview of the most widely used IMs and some more refined and newly developed ones follows in the next subsections. Since studies on the efficiency and sufficiency of different scalar and vector-valued IMs for several different structure types, including the NPPs have already been done, the observations and the conclusions, briefly reviewed in Sections 1.1. and 1.2. were used as a base for the selection of the IMs further considered in the scope of this study. Thus, the criteria for the selection of the considered IMs is also briefly provided in Section 2.

1.2. Overview of scalar ground motion intensity measures

Peak ground acceleration, PGA is probably the most commonly used IM in relation to seismic design and risk assessment of NPPs since the seismic hazard maps were mostly given in terms of PGA. It might be a suitable IM for specific structures, such as very stiff structures where the maximum seismic force, which appears in the structure is very well correlated with the PGA. On the other hand, peak ground velocity, PGV is more suitable for structures with intermediate frequencies, where the damage depends on the energy dissipation. Furthermore, the peak ground displacement, PGD might be suitable for flexible structures, where the maximum displacement of the structure correlates with the maximum displacement of the foundation. Since PGD is obtained through double integration of accelerations, it is prone to many errors in the estimation and is thus not a commonly used IM. The aforementioned IMs are all non-structure-specific and were shown not to be the most efficient or sufficient. Some combinations of the mentioned IMs were also proposed, such as the PGA/PGV ratio (Elhout, 2020) or the simplified formulation of the predominant period T_p (Rathje et al.,1998).

Spectral measures evaluated at the fundamental period of the structure ($S_a(T_1)$, $S_v(T_1)$ and $S_d(T_1)$), which are structure-specific, were also commonly adopted. $S_a(T_1)$ has proven to be more efficient than the PGA (Shome et al., 1998), but for tall and long-period buildings and structures subjected to near-source ground motions $S_a(T_1)$ may not be neither sufficient nor efficient because it doesn't give information about spectral shape. Thus, the contribution of the higher modes and the period lengthening because of structural non-linearity are not accounted for (Shome and Cornell 1999; Luco and Cornell 2007).

The aforementioned IMs are widespread, practical, and easily obtainable, but the variability in the EDP-IM relationship can be significant. Thus, several improvements were proposed to account for the spectral shape and contribution of higher modes. To tackle this problem, Cordova et al. (2000) proposed a new two-parameter IM S^* that reflects both spectral intensity and shape and thus accounts for inelastic strength and stiffness degradation (period elongation). The added index reduces the record-to-record variability in the predicted response obtained from the inelastic time history analyses, reducing the number of records necessary to obtain a given confidence in the results. Later, Lin et al. (2011) proposed a modification of this IM by employing two separate parameters, namely S_{N1} and S_{N2}. S_{N1} takes into account the first mode vibrations and the period elongation during non-linear response, while S_{N2} is intended to account for the first and the second mode vibrations. The use of this IM was studied on RC frames with 4, 10, and 16 storeys, where the inter-storey drift was observed as an EDP. S_{N1} performed better with 4 storey frames and S_{N2} with 10 and 16-storey frames. It was concluded that the new IM is appropriate for frame structures without significant torsional effects. The benefits of this IM are that the attenuation relations may be simply derived from the existing attenuation relations for accelerations while explicitly taking into account the variables that have the largest effect on the seismic behaviour of frame buildings, i.e. the elongation of the first vibration period during non-linear response and the contribution of higher modes. The IMs proposed by Cordova et al. and Lin et al. both consider spectral information only at certain periods and thus lack more detailed information on spectral shape. To address this drawback, Bianchini et al. (Bianchini et al., 2009) proposed an IM where S_a is evaluated at several different values of T. The efficiency of this IM, when compared to $Sa(T)$ or PGA was better for frames with the considerable effect of higher modes. This IM was then further studied and modified by several authors (for example, see Eads et al., 2015).

The integration of spectral values over a range of periods was also proposed by several authors to better account for spectral shape. For example, Housner (1952) proposed the integration of a pseudo-spectrum velocity curve, denoted as the Housner intensity I_H. The proposed integration limits were 0.1 s and 2.5 s, which were also adopted by Von Thun et al. (1988), who proposed a similar IM called velocity spectrum intensity (VSI), integrating the velocity response spectrum. This IM was considered applicable when assessing the seismic response of earth and rockfill dams. Furthermore, Von Thun et al. introduced the acceleration spectral intensity (ASI), where the acceleration spectrum is integrated, which has proven to be more important in the context of response and design of short-period dams. The three mentioned IMs did not consider the structural damage accounting for period elongation. Thus, several modifications (leading to the introduction of $MVSI$, $MASI$ and MI_H) were proposed for changing

the integration limits to more structure-specific (e.g. Kappos, 1990; Matsumura, 1992; Martinez-Reuda, 1998).

Several scholars observed the strong influence of shaking duration on the response of the buildings (e.g. Bommer and Martinez Periera, 1999; Bommer et al., 2004; Chandramohan et al., 2016). Thus, several IMs have been developed, considering the duration of the ground motion. Most of them include a factor accounting for the significant duration of the ground motion, in the following equations denoted as t_d, which is the time difference between 5% and 95% of arias intensity (AI). Examples of such IMs are compound acceleration-related intensity (I_a), which is based on PGA, compound velocity-related intensity (I_v) and Fajfar intensity (Fajfar et al., 1990), which are both based on PGV and compound displacement-related intensity (I_d), which is based on PGD. To account for both the spectral shape as well as the duration of the GM in combination with the most commonly used (and often relatively efficient and sufficient) $S_a(T_1)$, Marafi et al. (2016) proposed a more refined intensity measure IM_{comb} and also presented the suitability of this IM through the evaluation of the characteristics presented in the previous section.

While the aforementioned IMs depend on spectral values, other IMs were developed that are based on accelerograms directly. Those are sometimes referred to as energy-based IMs. Examples of those would be the arias intensity (AI), the cumulative absolute velocity (CAV), and root-mean-square acceleration (a_{arms}), which can then be used when defining the characteristic intensity I_c. CAV is defined as the area under the absolute accelerogram and represents the continuous accumulation of acceleration in a ground motion, which is a useful measure of the onset of structural damage. Arias intensity is one of the cumulative ground motion IMs as it is based on the integration of the squared acceleration from the acceleration time history. It accounts for both the duration and the amplitude of the ground motion, and it stems from the assumption that the amount of damage experienced by a structure is proportional to the energy dissipated by the structure per unit weight during the overall duration of the motion induced on it by the earthquake. Analogously to the integration of the acceleration, the velocity can also be integrated to obtain the cumulative absolute displacement (CAD). By multiplying the terms in the equation of motion by differential increments of displacements and performing integration, additional IMs, that can also be considered energy-based can be obtained. The final terms of the derived equations can be observed in Table 5, i.e. the relative input energy (E_{Ir}) and the absolute input energy (E_{Ia}). From those, additional IMs, namely relative input equivalent energy VSI ($V_{EIr}SI$) and absolute input equivalent energy VSI ($V_{EIa}SI$), can be obtained by integration of the energy response spectra in the period range from 0.1s to 3s. Those were then further modified to become more structure-specific by changing the integration interval boundaries, developing $MV_{EIa}SI$ and $MV_{EIr}SI$.

Recently, more advanced IMs for seismic collapse estimation have been proposed, an example of that being the filtered incremental velocity $FIV3$ (Dávalos and Miranda, 2019), which is evaluated using the area under a small number of acceleration pulses (time-domain features from an acceleration time series). It is period-dependent and represents the sum of the three largest incremental velocities obtained from a low-pass filter ground acceleration time series. The authors (Dávalos and Miranda, 2019) evaluated its efficiency and sufficiency, observing the response of a 4-storey RC frame, comparing the results with some other IMs (i.e. S_a, $S_a + \varepsilon$, $S_a + \eta$, IV, S_{aavg}, and IM_{comb}) and obtained promising results

Several studies have already been conducted regarding the suitability of different IMs. Rezaeemanesh and Mashayekhi (2022) studied the correlation between the PGA/PGV intensity measure and other ground motion IMs (AI, CAV, I_H, $A95$, T_m, T_P, DI, N_{cy}, I_p, $S_{a,avg}$) and realised that the best correlation was obtained between the PGA/PGV and the mean period T_m. Thus, this parameter could be employed for record selection as a frequency content-based parameter. Alzate and Hurtado (Alzate and Hurtado, 2021) studied the efficiency of IMs considering both near- as well as far-fault ground motion records and concluded that the velocity-based IMs have higher efficiency than acceleration-based, especially when the basic IMs (namely PGV and a_{rms}) are combined with the effective duration (t_d). This is shown through the observed effectiveness of the Fajfar intensity (Fajfar et al., 1990) and the characteristic intensity. Similar observations about the effectiveness of the velocity-based IMs for the estimation of the response of different types of structures were also made by other authors (e.g., see Zhang et al., 2017; Dávalos and Miranda 2019; Vargas-Alzate et al., 2021).

Sufficiency and efficiency-based rankings of IMs were also performed by Ebrahimian et al. (2015) and Burrati (2012). Burrati showed that the acceleration-based IMs perform better for short-period structures, while the velocity and displacement-based were deemed more appropriate for structures with longer vibration periods. Ebrahimian et al. observed several different EDPs and structures with different isolation systems and realised that the suitability of IMs depends on the type of the observed structure and isolation system. Nonetheless, acceleration IMs are still more commonly used.

Several authors also studied the suitability of different IMs for the NPP structures. Kim et al. (2022) conducted fragility analyses based on 30 recorded ground motions and performed correlation analyses between the fragility parameters and ground motion characteristics to investigate the ground motion variables that strongly affect the seismic capacity of the structure through observing the high confidence of low probability of failure (HCLPF) and the median capacity. Furthermore, the coefficients of variation were calculated for all of the important parameters. Kim et al. investigated 21 parameters: PGA, PGV, PGD, PGV/PGA, $Sa(T_n,\xi)$, I_a, a_{rms}, v_{rms}, d_{rms}, I_c, SED, CAV, ASI, VSI, I_H, SMA, SMV, AD, A_{95}, T_p and t_d. They observed that the highest correlation between the median capacity and the IMs was for SMA (based on the R^2 value), followed by ASI, RMS, AI and CAV, where higher values of those IMs resulted in lower median capacity. The correlation between the significant duration and the median capacity was observed to be unexpectedly weak. Since all of the studied ground motion records shared similar ranges of SMA and ASI, those parameters were regarded as the most strongly correlated with the median capacity since the wider ranges of other IMs didn't show any significant correlation with the observed capacity. For HCLPF, similar trends were observed. The effects of randomness and uncertainties were also studied, where it was concluded that the COVs of the measures of the uncertainties, namely β_R and β_U were lower than the ones of median capacity and the HCLPF, which means that the randomness and the uncertainty of the fragility curves do not appear to vary significantly with ground motion parameters, compared to the median capacity and the HCLPF. They thus concluded that except for the SMA, which showed the highest correlation with both the median capacity and the HCLPF, most of the earthquake characteristics are weakly correlated with the fragility parameters. Thus, with future study of this correlation and careful consideration of SMA, highly reliable seismic fragility curves with lower uncertainties using a reasonable number of ground motions could be developed.

A similar selection of the IMs was included in research by Nguyen et al. (Nguyen et al., 2021), where they studied their efficiency for seismic performance and fragility evaluations of the reactor containment building. Authors concluded that for the development of probabilistic seismic demand models, the IMs, directly related to acceleration, proved to be the most efficient, while the displacement and the velocity-based were less efficient. In another study, they identified the IMs that are strongly correlated to seismic responses of NPP structures (Nguyen et al., 2020), where they considered the low-frequency and high-frequency ground motions separately, observing several EDPs on both base-isolated and non-base-isolated numerical models of NPP structures. The results have shown that for the non-isolated structures subjected to low-frequency ground motions, the most suitable IMs are PGA, A_{95} and SMA, while if subjected to high-frequency ground motions SED, I_c and I_a preformed better. For base-isolated NPP structures SED, I_c, and I_a proved to be the most strongly correlated parameter with the seismic response for both types of ground motions. Since the results of the presented studies revealed that the suitability concerning the efficiency and the sufficiency of various IMs is case-specific, it makes sense to perform an efficiency analysis to choose the appropriate IM for the case studies presented in this deliverable. Some of the scalar IMs are listed in the following tables (Tables 1-7), and the criteria for the selection and the selection of the considered IMs are presented in Section 2.

Table 1: Non-structure-specific acceleration-related scalar intensity measures.

Acceleration-related	
Intensity Measure	**Name/reference**
$PGA = max\ (\lvert a(t) \rvert)$	Peak ground acceleration
$SMA = the\ 3rd\ highest\ PGA$	Sustained maximum acceleration (Nuttli, 1979)
$AI = \frac{\pi}{2g}\int_0^{t_f}(a(t))^2 dt,$ where t_f is the total duration of the GM	Arias intensity (Arias, 1970)
$CAV = \int_0^{t_f}\lvert a(t) \rvert dt,$ Where t_f is the total duration of the GM	Cumulative absolute velocity (Benjamin, 1988)
$I_a = PGA \cdot {t_d}^{1/3},$ where $t_d = t_{(95\%AI)} - t_{(5\%AI)}$	Compound acceleration-related intensity (Riddell and Garcia, 2001)
$I_c = (a_{rms})^{3/2} \cdot \sqrt{t_d}$ where $t_d = t_{(95\%AI)} - t_{(5\%AI)}$ and $a_{rms} = \sqrt{(\frac{1}{t_d})\int_{t_{(5\%AI)}}^{t_{(95\%AI)}}(a(t))^2 dt}$	Characteristic intensity (Park et al., 1985)

Table 2: Non-structure-specific velocity-related scalar intensity measures.

Velocity-related	
Intensity Measure	**Name/reference**
$PGV = max\ (\lvert v(t) \rvert)$	Peak ground velocity
$SMV = the\ 3rd\ highest\ PGV$	Sustained maximum velocity (Nuttli, 1979)
$FI = PGV \cdot t_d^{0.25},$ where $t_d = t_{(95\%AI)} - t_{(5\%AI)}$	Fajfar intensity (Fajfar et al., 1990)
$CAD = \int_0^{t_f} v(t) dt,$ where t_f is the total duration of the GM	Cumulative absolute displacement (Mackie and Stojadinović, 2001)
$I_v = PGV^{2/3} \cdot t_d^{1/3}$	Compound velocity-related IM (Riddell and Garcia, 2001)
IV	Incremental velocity, i.e. the area under the maximum acceleration pulse (Anderson and Bertero, 1987)
$SED = \int_0^{t_f}(v(t))^2 dt$	Specific energy density (Kramer, 1996)

Table 3: Non-structure-specific displacement-related scalar intensity measures.

Displacement-related	
Intensity Measure	**Name/reference**
$PGD = max\ (\lvert u(t)\rvert)$	Peak ground displacement
ID	Incremental displacement, i.e. the area under the maximum velocity pulse (Anderson and Bertero, 1987)
$I_d = PGD \cdot t_d^{1/3}$	Compound displacement-related IM (Riddell and Garcia, 2001)

Table 4: Some of the remaining non-structure-specific scalar intensity measures.

Other	
Intensity Measure	**Name/reference**
$PGV/PGA = \frac{\max\ \lvert v(t)\rvert}{\max\ \lvert a(t)\rvert}$	Peak ground velocity and peak ground acceleration ratio (Kramer, 1996)
$T_p = 4.3PGV/PGA$	The predominant period (Kramer, 1996)
$T_m = \frac{\sum C_i/f_i}{\sum {C_i}^2}$, where f_i denotes the discrete Fourier transform of frequencies ranging from 0.25 to 20 Hz, and C_i denotes the Fourier amplitudes	The mean period (Rathje et al., 1998)

Table 5: Structure-specific spectral intensity measures.

Spectral	
Intensity Measure	**Name/reference**
$Sa(T_n, \xi) = max(\lvert \ddot{u}_t(t, T_n, \xi)\rvert)$, Where $\ddot{u}_t = \ddot{u} + \ddot{u}_g$ is the total acceleration	Spectral Acceleration (Chopra, 2007)
$Sa(T_1)$	Spectral acceleration at T_1 (Shome et al., 1998)
$E_{Ir} = E_{kr} + E_d + E_s = -\int_0^{t_f} m \cdot \ddot{u}_g(t) \cdot \dot{u}_r(t) \cdot dt$, Where m is the mass of the system (viscous damped SDOF system), $\ddot{u}_g(t)$ represents the ground acceleration time history and $\dot{u}_r(t)$ relative velocity time history of SDOF ($\xi = 5\%, T$) model	Relative input energy (Uang and Bertero, 1990)
$E_{Ia} = E_{ka} + E_d + E_s = \int_0^{t_f} m \cdot \ddot{u}_t(t) \cdot \dot{u}_g(t)\ \cdot dt$, Where m is the mass of the system (viscous damped SDOF system), $\dot{u}_g(t)$ is the relative velocity time history and $\ddot{u}_t(t)$ the absolute acceleration time history of SDOF ($\xi = 5\%, T$) model	Absolute input energy (Uang and Bertero, 1990)

Table 6: Structure-specific integral intensity measures.

Integral	
Intensity Measure	**Name/reference**
$ASI = \int_{0.1}^{0.5} S_{pa} dT$	Acceleration spectrum intensity (Housner 1952; Thun et al., 1988)
$VSI = \int_{0.1}^{2.5} S_v dT,$ where S_v is the velocity spectrum with 5% damping	Velocity spectrum intensity (Housner 1952; Thun et al., 1988)
$DSI = \int_{2.0}^{5.0} S_d(T, 5\%) dT,$	Displacement spectrum intensity (Bradley, 2011)
$I_H = \int_{0.1}^{2.5} S_{pv} dT,$ where S_{pv} is the velocity spectrum with 5% damping	Housner intensity (Housner, 1952)
$V_{EIr}SI = \int_{0.1}^{3.0} V_{EIr}(T) dT = \int_{0.1}^{3.0} \sqrt{\frac{2E_{Ir}}{m}} dT$	Relative input equivalent energy VSI (Decanini and Mollaioli 1998; 2001; Chou and Uang, 2000; Cheng et al., 2015)
$V_{EIa}SI = \int_{0.1}^{3.0} V_{EIa}(T) dT = \int_{0.1}^{3.0} \frac{\sqrt{2E_{Ia}}}{m} dT$	Absolute input equivalent energy VSI (Decanini and Mollaioli 1998; 2001; Chou and Uang, 2000; Cheng et al., 2015)
$MASI = \int_{0.5T}^{1.25T} S_{pa} dT$ *various integration limits may be found in the literature	Modified ASI (Kappos, 1990; Matsumura, 1992; Martinez-Reuda, 1998)
$MVSI = \int_{0.5T}^{1.25T} S_v dT$ * various integration limits may be found in the literature	Modified VSI (Kappos, 1990; Matsumura, 1992; Martinez-Reuda, 1998)
$MI_H = \int_{0.5T}^{1.25T} S_{pv} dT$ * various integration limits may be found in the literature	Modified IH (Kappos, 1990; Matsumura, 1992; Martinez-Reuda, 1998)
$MV_{EIr}SI = \int_{0.5T}^{1.25T} \frac{\sqrt{2E_{Ir}}}{m} dT$	Modified $V_{EIr}SI$ (Avşar and Ozdemir, 2013)
$MV_{EIa}SI = \int_{0.5T}^{1.25T} \frac{\sqrt{2E_{Ia}}}{m} dT$	Modified $MV_{EIa}SI$ (Avşar and Ozdemir, 2013)

Table 7: Multi-parameter intensity measures.

Multi-parameter	
Intensity Measure	**Name/reference**
$S^* = S_a(T_1) \cdot {R_{S_a}}^{\alpha}$, where $R_{S_a} = \frac{S_a(T_f)}{S_a(T_1)}$ and the combination of $T_f = 2T_1$ and α=0.5 was proposed as optimal	(Cordova et al., 2000)
$Sa_{avg}(\boldsymbol{T}^*) = Sa_{avg}(T^{(1)}, \dots, T^{(n)}) = (\prod_{i=1}^{n} S_a(T^{(i)}))^{1/n}$, where $\boldsymbol{T}^* = [T^{(1)}, \dots, T^{(n)}]$ represents a vector of n periods of interest, Sa_{avg} is the geometric mean of $S_a(T^{(i)})$, and n should represent at least 10 logarithmically-spaced points. Two different period-intervals were suggested in the literature: $\boldsymbol{T}_1^* = [T_1, \dots, 2T_1]$ for first-mode dominant (low period) structures and $\boldsymbol{T}_2^* = [0.2T_1, \dots, 2T_1]$ for medium-to-long period structures affected by higher modes. Eads et al. later proposed the interval from $0.1T_1$ to $3T_1$ with a uniform spacing of 0.1s for collapse assessment.	Average spectral acceleration (Vamvatsikos and Cornell, 2005), (Bianchini et al., 2009), (Eads et al., 2015)
S_{N1}, S_{N2} $S_{N1} = S_a(T_1)^{\alpha} \cdot S_a(CT_1)^{1-\alpha}$ $S_{N2} = S_a(T_1)^{\beta} \cdot S_a(T_2)^{1-\beta}$, where C is a constant taking into account the period elongation with the limit values of 1.0 (elastic response) and 2. The value of $C = 1.5$ was proposed by the authors for RC frames, which is also used in the ASCE/SEI 7-05 Standard (ASCE 2006) as a period elongation factor. The authors found $\alpha = 0.5$ and $\beta = 0.75$ to be the optimal values for RC frames.	(Lin et al., 2011)
$FIV3 = \max\left\{\begin{matrix} V_{s,max1} + V_{s,max2} + V_{s,max3,} \\ \left\|V_{s,min1} + V_{s,min2} + V_{s,min3,}\right\| \end{matrix}\right\}$ $V_s(t) = \left\{\int_t^{t+\alpha T_n} \ddot{u}_{gf}(\tau)d\tau, \forall t < t_{end} - \alpha T_n\right\}$, where t_{end} is the last time instance of the GM, $\ddot{u}_{gf}$ is the low-pass filtered acceleration curve (e.g. 2nd order Butterworth low-pass filter), α is a scalar proportionality factor, which can be considered structure and data set dependant and T_n the natural vibration period of the SDOF system.	(Dávalos and Miranda, 2019)

(Continued on next page)

Table 8: Multi-parameter intensity measures (continued from previous page).

$$IM_{comb} = S_a(T_n) IM_{dur}^{C_{dur}} IM_{shape}^{C_{shape}}$$ where: $$IM_{shape} = S_a(T_n, \alpha) = \frac{\int_{T_n}^{\alpha T_n} S_a(T) dT}{S_a(T_n)(\alpha - 1)T_n}$$ IM_{dur} Is the significant duration computed as the time interval, for example, between 5% and 95% of the maximum. C_{dur} and C_{shape} are empirical exponents accounting for the structure's sensitivity to IM_{dur} and IM_{shape}. Parameter α takes into account the period elongation and was proposed to be $\alpha = C_\alpha \sqrt{\mu}$, where the authors used the value of $C_\alpha = 1.3$ and μ is the system's displacement ductility factor.	(Marafi et al., 2016)
$$I_{Np} = S_a(T_1) {N_p}^{\alpha},$$ where N_p accounts for the spectral shape and is determined as: $$N_p = \frac{1}{T_1 Sa(T_1)} \int_{T_1}^{T_N} Sa(T) dT \approx \frac{Sa_{avg}(T_1, \dots, T_N) \cdot (T_N - T_1)}{T_1 Sa(T_1)}$$ or $$N_p = \frac{Sa_{avg}(T_1, \dots, T_N)}{Sa(T_1)}$$ And the optimal range of α is between 0 and 1 and accounts for different weights to the contribution of the spectral accelerations beyond the first mode compared to the spectral value at T_1. The value of $\alpha = 0.4$ was proposed by Bojórquez and Iervolino	(Bojórquez and Iervolino, 2011)

1.3. Overview of vector-valued ground motion intensity measures

The scalar IMs are simple measures of ground motions that can be easily applied in studies. Additionally, the conventional PSHA is performed for the scalar IMs, commonly for PGA and S_a at various vibration periods. However, their drawback is they represent only a fragment of information about the complex time history of ground motions, which means that a single IM cannot predict ground motions for all possible needs. As a consequence, the aim of many scholars has been to propose vector-valued IMs, usually with a primary IM and a secondary IM that account for some additional characteristics of ground motions that cannot be captured by the primary IM. In general, vector-valued IMs can be defined by a combination of the listed IMs from Chapter 1.1. Some of the more common ones are listed in Table 8 along with some additional IMs.

Most of the vector-valued IMs considered in the literature consist of a combination of $S_a(T_1)$, with one or more additional parameters that account for the spectral shape. Considerable research has been done to analyse the use of vector-valued IMs with the aim of selecting the most appropriate combination of the parameters to reduce the uncertainties in the seismic response of structures and thus improve the efficiency of the analysis (e.g., see Baker and Cornell, 2006; Bojórquez et al., 2008; Yakhchalian et al., 2015; Zhou et al., 2017; Zavala et al., 2023). If using a two-component vector, the second component can be a ratio of two scalar IMs. This usually improves the efficiency of the IM, compared to that based on a given scalar IM.

There are different approaches to scaling the ground motion. The most common one, when preforming analysis using a two-component vector is to scale the ground motion to the level of the first component, usually deemed as the predominant and then preform logistic regression analysis for the second component and the observed EDP to determine the fragility functions. Alternative approach that simplifies this analysis is to make a selection of ground motions based on the first component of the vector-valued IM (without any scaling of the ground motions introduced) and then the seismic assessment by using the other component as a scalar IM. The aim when synthesising a vector IM is to increase the information about the ground motion without making the analysis process too complex. This can be evaluated through the efficiency and sufficiency of the IMs, where the sufficiency is usually estimated using the concept of relative entropy. Jayaler et al. (2012) proposed a so-called relative sufficiency measure (RSM), which is meant to measure the relative efficiency of one IM with respect to another and can be explained as the information gain or entropy between two PDFs.

Intuitively it could be argued that the efficiency of the vector IMs in terms of conditional seismic demand prediction is high, the inclusion of additional elements in vector IMs also increases the uncertainty of the IM, which increases the uncertainties in the estimation of EDPs. Furthermore, the studies by Rajeev et al. (2008) and Zelachi et al. (2017) resulted in the conclusion that the vector IMs provide negligible improvements in EDP estimates compared to the scalar ones. Li and Cai (2022) further investigated the effect of uncertainties and realised that while the implementation of vector IMs reduces the epistemic uncertainties, it increases the aleatory uncertainties. They conducted research employing the Monte Carlo simulation, which demonstrated that the use of vector IMs did not significantly improve the accuracy of the PSDA, especially when the structural effect was not considered. Thus, they highlighted that if the structural collapse effect is not considered, scalar IMs are preferred. The use of vector IMs is beneficial when the structural effect is considered, and the collapse of structures is notably better predicted by the vector IMs. To conquer these obstacles, keeping the simplicity of the analysis using the scalar IM, while also including the benefits of newly developed vector IMs, Bojorquez et al. (2011) proposed the I_{Np} intensity measure (note that since it is a scalar IM, it is listed in the previous section) and proved its efficiency in comparison to the equivalent vector IM.

Considering all the aforementioned pros and cons of employing a vector IM in comparison to a scalar one, it could be argued that the choice of the appropriate IM is case-specific (since the results of studies were based on different structural types, fault types, and observed EDPs) and usually relies on the balance between enhanced performance and available information.

Table 9: Some of the commonly used vector-valued intensity measures, found in the literature.

Vector-valued IMs	
Intensity Measure	**Name/reference**
$[PGA, M]$, Where M is the moment magnitude of the event generating ground motion	Elefante et al. 2010
$[S_a(T_1), R_{T_1,T^*}]^b$, Where $R_{T_1,T^*} = \frac{S_a(T^*)}{S_a(T_1)}$ and $T^*$is suppose to capture the important characteristics of the shape of the spectrum, thus two values are usually considered: $T_1^* = T_1$ and $T_2^* = T_2$	Baker and Cornell (2008a, b)
$[S_a(T_1), \varepsilon(T_1)]$, Where ε is a measure of the spectral shape accounting for the number of standard deviations by which a given $lnS_a(T_1)$ value differs from the mean predicted $lnS_a(T_1)$ considering a given magnitude M, distance R and other properties denoted by φ. $\varepsilon(T_1) = \frac{lnS_a(T_1) - \mu_{lnS_a(T_1)}(M,R,\varphi)}{\sigma_{lnS_a(T_1)}(M,R,\varphi)}$	Baker and Cornell (2006)
$[S_a(T_1), R_{T_1,T^*}, \varepsilon(T_1)]^b$	Baker and Cornell (2008a)
$[S_a(T_1),\ N_p]$, Where N_p accounts for the spectral shape and is determined as: $N_p = \frac{1}{T_1 Sa(T_1)} \int_{T_1}^{T_N} Sa(T)dT \approx \frac{Sa_{avg}(T_1,\dots,T_N)\cdot(T_N - T_1)}{T_1 Sa(T_1)}$ or $N_p = \frac{Sa_{avg}(T_1,\dots,T_N)}{Sa(T_1)}$	(Bojorquez et al., 2008) (Bojórquez & Iervolino, 2011)
$[S_a(T_1), S_a(2T_1), \beta/S_a(T_1)]$, Where $\beta/S_a(T_1)$ takes into account the shape of the spectra, can be denoted as θ and expressed as: $\theta = \delta + \frac{1}{3}\frac{(1-\delta)(2+\delta)}{(1+\delta)}$ and $\delta = \frac{Sa(2T_1)}{Sa(T_1)}$	(Nicknam et al., 2015)

2. Selection of scalar and vector intensity measures for the case studies

Seismic fragility assessment of SSCs can be approached through various methodologies. As discussed in Section 1, numerous scalar and vector IMs are available for this analysis. However, the seismic fragility and risk analysis are not only affected by the choice of IMs but are also dependent on the ground motion records used to assess the structure's response and the seismic analysis type. Consequently, the ground motion selection process is often constrained by Multiple Stripe Analysis (MSA, e.g., see Jalayer, 2003) and Incremental Dynamic Analysis (IDA; Vamvatsikos and Cornell, 2002), which are commonly employed seismic analysis methods. In MSA, a conditional spectrum (CS) is utilized, conditioned on the chosen IM, and ground motion records are selected or simulated to match the CS. The development of the conditional spectra and the selection of the corresponding ground motion records for the METIS case study is presented in Deliverable 5.2 (Šipčić et al., 2023). This approach guarantees the hazard consistency of the ground motion records for seismic analysis. Conversely, IDA involves selecting a set of ground motion records from established databases, considering site-specific characteristics, and scaling them based on the chosen IM.

The outcomes of seismic fragility analysis inherently depend on the structural model employed. Various structural models can be utilized for the analysis. For critical structures such as Nuclear Power Plants (NPPs), the inclusion of soil-structure interaction is very important. Therefore, the type of structural model serves as a parameter that can influence conclusions regarding studies aimed at selecting the optimal ground motion IM. Another influential factor affecting the outcome of studies aimed at selecting the optimal IM is the Engineering Demand Parameter (EDP), which typically defines the limit states of the SSCs.

Currently, the most widely used IM is the Peak Ground Acceleration (PGA) for both existing buildings and Nuclear Power Plants (NPPs). However, despite its conventional usage, numerous studies, as discussed in Section 1, suggest that PGA may not be the most suitable IM for all structures. Given the complexity of NPP structures, consisting of SSCs with diverse dynamic characteristics and varying sensitivity to different EDPs, the performance of PGA alongside other IMs was evaluated through the design of three case studies, as summarized in Table 9.

The case studies employed three distinct seismic fragility analysis approaches: IDA, CS-MSA approach and the CS-cloud approach. In the latter case, the resulting IM-EDP pairs were subjected to linear regression in the log-normal space, also known as cloud analysis (e.g., see Zentner, Gündel and Bonfils, 2016), in two out of the three case studies. Diverse EDPs were observed for the studied components, with one study focusing on floor spectral acceleration at various elevation levels, while the other two studies concentrated on ultimate displacement. The fragility resulting specific to each component and associated dispersion was evaluated to identify the optimal combination of conditioning IM and analysis approach. Additionally, refined and simplified Soil-Structure Interaction (SSI) models were considered, along with numerous hazard-consistent ground motion record sets.

In the subsequent sections, detailed descriptions of Case Studies 1, 2, and 3 are provided, followed by the presentation and discussion of the obtained results.

Table 9: A summary of case studies.

SUMMARY OF THE CASE STUDIES		
CASE STUDY 1	**CASE STUDY 2**	**CASE STUDY 3**
Section 3	Section 4	Section 5
SCALAR INTENSITY MEASURES		
PGA **Sa(0.10 s)** **Sa(0.15 s)** **Sa(0.20 s)** **AvgSa(0.10-0.40 s)** AvgSa(0.10-0.20 s) AvgSa(0.05-0.15 s)	PGA Sa(0.1 s) AvgSa(0.1s-0.4 s)	PGA Sa (0.26 s)
GROUND MOTIONS AND SEISMIC ANALYSIS		
IDA (two-stage approach, with linear analysis to obtain the acceleration time histories of the reactor floor, which were used for IDA for the component with a set of 105 two-component ordinary GMRs from PEER database, with M>6.2, PGA>0.14g).	CS-MSA (30 hazard-consistent GMRs for each IML, criteria of $V_{s,30}$>400 m/s and GMRotD50; mean and dispersion of the fragility curve determined with maximum likelihood method). IDA (30 GMR pairs, characterised as ordinary, from NGA-West2 database consistent with hazard for Greece; mean and dispersion of fragility determined with the method of moments).	CS-MSA (hazard consistency in the horizontal spectral using the sets of GMRs selected in WP5). Cloud analysis (linear regression in lognormal space with the IM-EDP pairs from the CS-MSA analysis).
SSI MODEL		
The simplified structural model as developed by EPRI (2007) was established in OpenSees (OpenSees, 2006), a simple mass-spring damper system was employed to model the soil-structure interaction. The service water pump component model studied as proposed by EPRI (2018), involves adjusting the stiffness to obtain a set of components with various fundamental periods.	Same as for Case study 1.	NPP Reactor building developed in the METIS project, built in Salome-meca and Code-Aster. The soil-structure interaction and site response was taken into account. Transfer functions were calculated and used to analyse the response of the model at different locations throughout the reactor building.
EDP / limit-state EDP		
The maximum value (over time) of the geometric mean of the X and Y displacement time histories. Limit-state displacement (d_u=2.9 mm).	The maximum value (over time) of the geometric mean of the X and Y displacement time histories. Limit-state displacement (d_u=2.9 mm).	The floor spectral acceleration averaged over the frequency band of interest (5Hz-9Hz) for the equipment considered (switchgear), the maximum floor spectral acceleration over all three directions is used to compute the average. The EDP is considered at four selected elevation levels.

3. CASE STUDY 1: Optimality of GMM-relevant scalar IMs for the AP1000 reactor model via generic ground motions

The selection of the most suitable IM within the nuclear industry is a multifaceted decision influenced by the particular project's goals and the surrounding context. The determination of the appropriate intensity measure relies on several key factors, including the outcomes of a thorough seismic hazard analysis, site-specific conditions, and compliance with the engineering standards and guidelines specifically tailored to the nuclear sector within a given region. Although Peak Ground Acceleration (PGA) stands as the prevalent choice for measuring intensity of the ground motion records within the nuclear industry, the subsequent section delves into a more extensive selection of scalar IMs. This involves PGA, Sa(T, 5%) and AvgSa, all of which are checked for their optimality in assessing the service water pump seismic fragility.

3.1. Reactor building

The structure under study is the main containment/auxiliary building based on the AP1000 advanced reactor design. The AP1000 is an advanced pressurized water reactor (PWR) nuclear power plant design that was developed by Westinghouse Electric Company. The structural model, formed using OpenSees (OpenSees, 2006), consists of three concentric sticks (Willaume & Noret, 2011). The sticks represent the Coupled Auxiliary and Shield Building (ASB), the Steel Containment Vessel (SCV), and the Containment Internal Structure (CIS). ASB is a part of a nuclear reactor building that houses auxiliary systems, such as pumps, valves, and electrical equipment, as well as a shield wall that helps protect the reactor from radiation and it is usually located adjacent to the reactor containment structure. SCV is a large, steel structure that surrounds the reactor pressure vessel and provides an additional layer of protection against the release of radioactive materials. CIS, on the other hand, is a system of structural components and support systems that are located within the SCV and help to support the reactor pressure vessel and associated systems. The three sticks are horizontally separated in Figure 3 (right), with a concentric and structurally independent arrangement, where each stick consists of discrete masses are connected via elastic beams. The modelling data are taken from the Electrical Power Research Institute (EPRI, 2007). More specifically, the bottom elevations of ASB, SCV, and CIS are 18.44 m, 30.48 m, and 18.44 m in the respective order, and their total heights are 83.10 m, 55.44 m, and 33.07 m. The total mass of the AP1000 is 1.5×10^5 tons; the mass ratio of ASB, SCV, and CIS relative to the entire model is 86%, 3%, and 11%, respectively. Also, Rayleigh damping of 7% (ASCE, 2019) is applied to the 1st and 3rd SSI modes with periods of 0.46s and 0.30s.

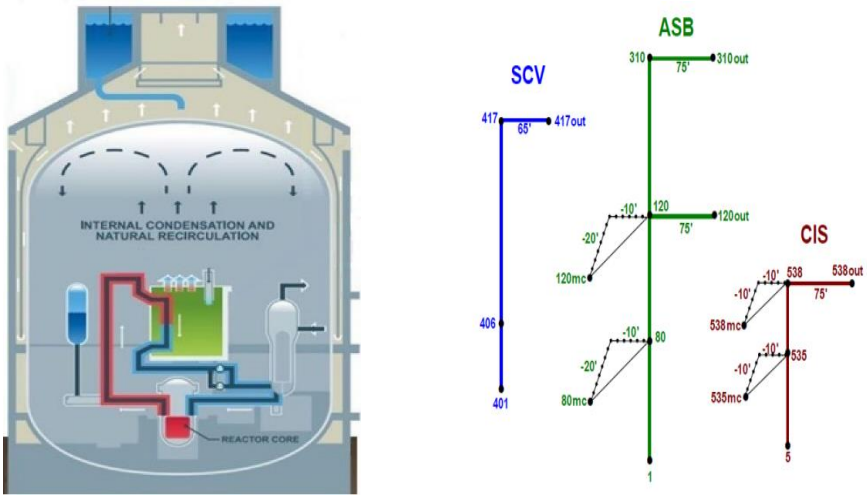

Figure 3: Drawing of the AP1000 reactor design (left) and model of simple sticks (right) per EPRI (2007).

It should be noted that the EPRI model also includes massless outrigger nodes connected to the centerline by rigid links at the top of the auxiliary building, steel containment vessel, and containment internal structure. Mass centers have been offset from the shear center at locations in the auxiliary building and the CIS to introduce natural torsion into the models. The shear centers of the three sticks are coincident along the Z-axis.

The fundamental period of the reference structure, as determined from the modal analysis, is 0.26 s. The three substructures exhibit semi-independent vibration behavior, where they are connected at the base and do not significantly influence each other; the ASB tower contributes more significantly to the observed vibrational movement of the entire structure.

3.2. Soil structure interaction

Integrating soil-structure interaction (SSI) is a fundamental aspect when evaluating the seismic safety of a nuclear power plant. By incorporating SSI into the design process, it allows for the appropriate engineering of the plant's structures and systems, ensuring their ability to withstand anticipated seismic threats. Failing to account for SSI can result in an underestimation of the seismic risk.

A simple cone model is utilized to replicate the interaction between the soil and the structure-foundation system. The first attempt to create a simple physical model of soil can be traced back to Ehlers (1942) and subsequently Wolf (1998), who employed a truncated semi-infinite cone to depict the movements of a foundation located on an elastic half-space. Various examples of cones representing vertical, horizontal, rocking, and torsional degrees of freedom are presented in Figure 4. According to Wolf, for all components of motion, a rigid basemat, on the surface of a homogeneous soil halfspace with Poisson's ratio ν, can be modeled as a truncated semi-infinite cone of equivalent radius r_0, apex height z_0 and wave velocity C. For the horizontal and torsional cones deforming in shear the appropriate wave velocity C equals the shear-wave velocity C_s. For the vertical and rocking cones deforming axially, C equals the dilatational-wave velocity C_p for $\nu \leq 1/3$ and is limited to $2C_s$ for $1/3 < \nu \leq 1/2$.

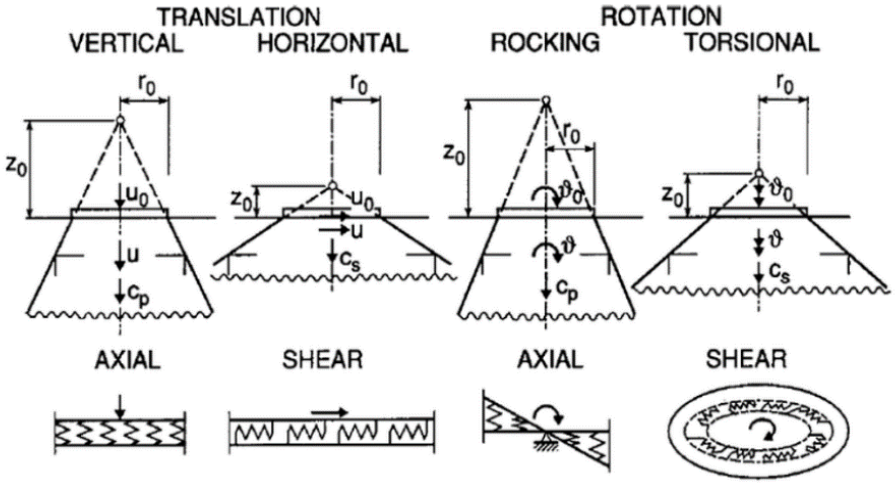

Figure 4: Cones for different degree of freedoms (adopted from Wolf, 1998)

From a modelling perspective, the cone is depicted as a simplified mass-spring-damper system. This model assumes that the soil can be approximated as a linear elastic medium with consistent stiffness throughout its depth. The foundation of the structure is depicted as a rigid mass connected to the soil through a spring and a dashpot. The spring characterizes the soil's stiffness, while the dashpot represents the soil's damping properties. The analysis employs a rectangular foundation with dimensions of 65x45 m. Additionally, the soil behavior is simulated using a shear wave velocity of 350 m/s and a density of 2 Mgr/m^3. Considering the mass-spring-damper system for soil-structure interaction, the fundamental period of the power plant is determined to be 0.46s.

3.3. Service water pump

For the purpose of conducting a component reliability analysis, a service water pump (EPRI, 2018) is used as a case study. The service water pump is a long column vertical pump that is anchored to the concrete operating floor of the pump structure (Figure 5). The pump column, pump shaft, motor stand, and motor are modelled as beams. According to EPRI (2018) report, the translation of the pump motor is one of the most critical failure modes; therefore, the focus shifts to the motor stand. The motor stand has a cylindrical shape with two large windows cut out, resulting in two 120° arcs that act as guided cantilever beams in bending about the weak axis direction when lateral acceleration is applied to the motor. It is noted also that the analysis was based on different dimensions of the motor stand than the dimensions measured in the field. The analysis dimensions were smaller, resulting in a significantly more flexible motor stand. The simplified model used for the simulation is a three-dimensional stick, which incorporates a single mass situated at its upper end (Figure 6). It is assumed to be positioned on the top of the CIS tower. This may not necessarily represent a realistic configuration, yet this does not matter for the purposes of our study; we are only interested in checking different IMs against a system with plausible structural characteristics.

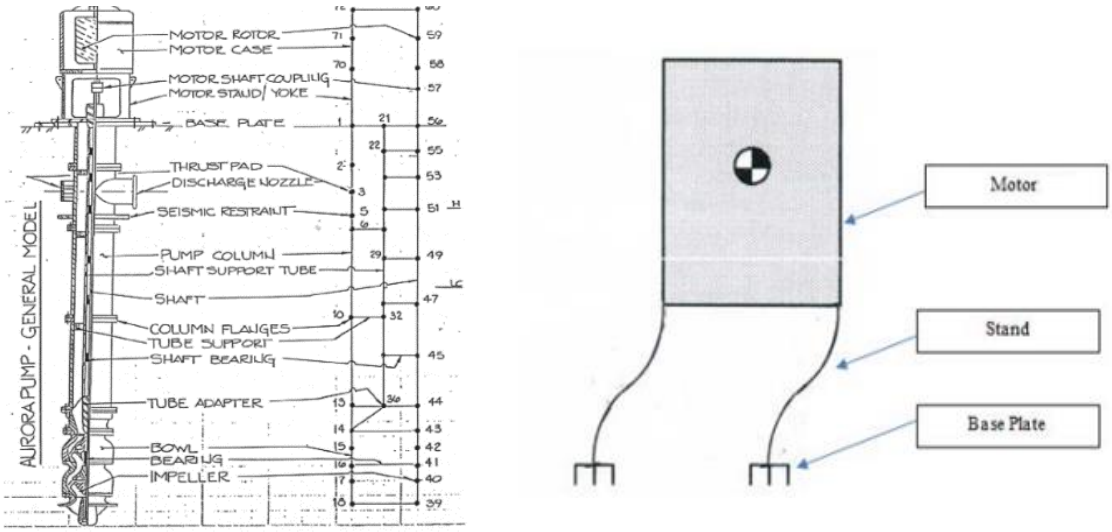

Figure 5: Schematic drawing of the service water pump (left) and simplified motor stand model per EPRI (2018) (right).

The pump's performance is characterized by an elastic-perfectly-plastic force-deformation backbone that ends at an ultimate ductility of 1.25 and exhibits moderately pinching hysteresis. The pump is symmetric in both principal axes X and Y and has a fundamental period of T_{pump} = 0.101 s and a yield strength of V_{yield} = 37.79 kN. A median damping ratio of ξ= 5%, typical for mechanical equipment (as stated in EPRI 2018), is adopted. Failure is assumed to take place at a maximum displacement of d_u = 0.0029 m for the pump, which is to be utilized as the capacity threshold for fragility analysis. Cyclic degradation of strength and stiffness is modeled via two damage parameters, specifically linked to ductility and energy, which have been introduced following the Hysteretic uniaxial material model of Scott & Filippou (2016). The first parameter adjusts the cyclic strength degradation (and stiffness) in proportion to the strain level, meaning that higher strain levels result in higher degradation. Conversely, the second parameter alters the cyclic strength (and stiffness) degradation in relation to the energy dissipated through inelastic strain, leading to an increase in strength reduction as the number of cycles at a constant strain level rises. Both parameters are set to a value of 0.10.

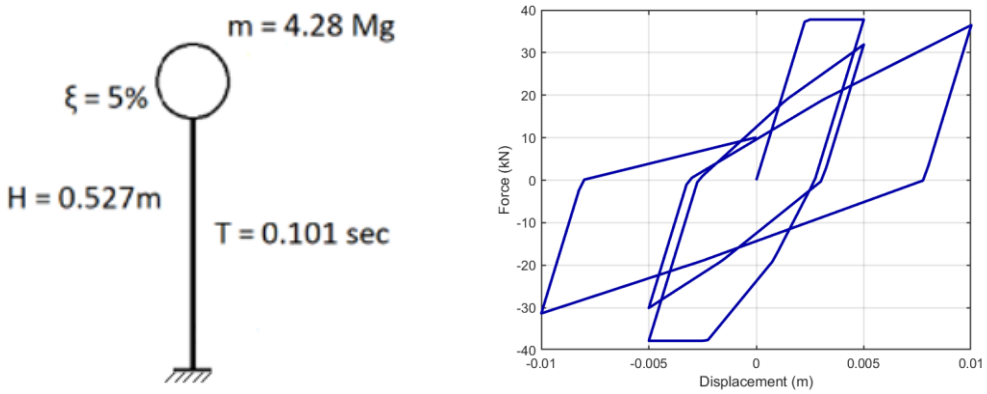

Figure 6: Pump motor stand simulation model (left) and hysteretic behavior of the model under static cyclic loading (right).

Using the fundamental model of the pump as the reference, the stiffness is adjusted while keeping the strength constant. This change in stiffness leads to a change in yield displacement, thereby generating virtual replicas of the same model with different fundamental eigenperiods; the eigenperiods span from 0.02 to 1.0 s. Again, the objective is not to capture actual components, but rather to generate a wide selection of realistic-looking components at different vibration frequencies. Figure 7 illustrates the schematic performance of the pumps in this approach.

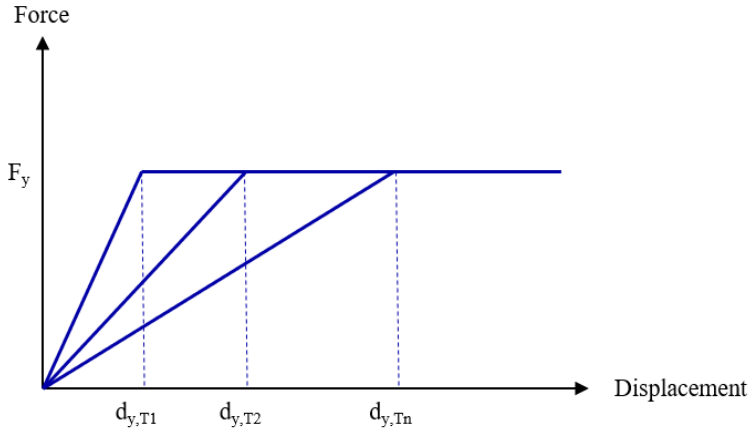

Figure 7: Capacity curves of pumps with different periods

3.4. Performance evaluation

Incremental Dynamic Analysis (IDA; Vamvatsikos and Cornell, 2002) is utilized to assess the performance of the reactor-pump system via response history analysis for different pump periods. A suite comprising 105 two-component ordinary (i.e., non-long-duration, non-pulse-like, firm-soil site) ground motion records is employed. They have been selected from the PEER database (Pacific Earthquake Engineering Research Center, 2005) from events with moment magnitude greater than 6.2, having PGA > 0.14 g, to comply with a high-seismicity site.

Given the minimal mass of the pump relative to the reactor building, a classic two-stage cascade approach is employed for the analysis. In the first stage, one linear response history analysis is carried out per ground motion for the reactor building, while also taking into account the soil-structure interaction effects. Under the assumption of linearity, which is valid for the simple model at hand, the resulting floor acceleration time histories can be scaled to obtain the response at different intensity levels of the scaled ground motions. In the second stage, the floor acceleration time histories can be employed as inputs to the pump model and can be scaled as needed to conduct IDA and assess the performance of the component.

Given the requirements presented in sub-section 1.1.2, three competing scalar IMs are considered. The first is Peak Ground Acceleration (PGA), which is widely used in the nuclear industry (Zentner et al., 2011). The second is the 5%-damped spectral acceleration at a specific period T, or Sa(T), which is deemed an appropriate index for first-mode-dominated linear or nonlinear structures (Shome & Cornell, 1999; Tavakoli & Pezashk, 2005; Abrahamson & Silva, 2008). Finally, the (geometric) average spectral acceleration (AvgSa) in distinct ranges of short periods (i. e. 0.05-0.15 s, 0.10-0.20 s and 0.10-0.40 s) is considered, as it has been demonstrated to deliver satisfactory performance for a variety of structures (Vamvatsikos & Cornell, 2005; Bojórquez & Iervolino, 2011; De Biaisio 2014, Eads et al., 2015; Kazantzi & Vamvatsikos 2015; Kohrangi et al. 2016a; Adam et al. 2017). To ensure consistency with ground motion models, the geometric mean of the horizontal ground motion components is utilized to define the IMs.

The displacement response of the 3D model of the service water pump comprises two horizontal components, namely X and Y. The Engineering Demand Parameter (EDP) employed to estimate the structural response of the model is determined by taking the maximum value (over time) of the geometric mean of the X and Y displacement time histories.

The IDA results are utilized to obtain fragility functions of the pump per Bakalis & Vamvatsikos (2018) using the so-called vertical statistics approach. For each IDA curve generated, the IM value corresponding to the given limit-state threshold of d_u = 0.0029 m is estimated. Lognormal fragility curves are estimated for PGA, spectral acceleration at the fundamental period of each replica of the component Sa(T1) and spectral acceleration at three alternative low periods: Sa(0.10 s), Sa(0.15 s), and Sa(0.20 s). Additionally, three distinct period ranges are considered for AvgSa fragility assessment: AvgSa(0.10-0.40 s), AvgSa(0.10-0.20 s), and AvgSa(0.05-0.15 s). Table 10a displays the median fragility values corresponding to the given IM and the period of the pump investigated, while Table 10b provides information about the fragility dispersions. Table 11 highlights the optimal IMs by denoting it in bold. This selection is made based on the lowest dispersion, with the exclusion of results associated with spectral acceleration at the fundamental period of each component.

In cases where the eigen period is less than 0.05 s and higher than 0.60 s, the PGA demonstrates the highest efficiency when used as the IM for fragility analysis of the pump. On the other hand, for all other cases, regardless of the period range used, AvgSa proves to be the most efficient IM. More specifically, for a period range between 0.05 and 0.10 s, AvgSa(0.05-0.15 s) exhibits the lowest dispersion. For periods ranging from 0.1 to 0.2 s the same pattern applies for both Sa(0.20 s) and AvgSa(0.1-0.2 s). Finally, AvgSa(0.1-0.4 s) is the optimal IM for all the periods from 0.25 to 0.55 s.

The preceding findings are also visually depicted in Figure 8 and Figure 9 In these visual representations, a red dashed line is used to illustrate the median or dispersion of the 5 %-damped spectral acceleration at the fundamental period of each analyzed component. It is evident that the spectral acceleration at the fundamental period of the component exhibits the least dispersion. However, it is also important to note that each non-structural component has its unique eigen period, ranging from a few milliseconds to over a second. This means that a single 'optimal' period for the analysis of the entire structure may not exist. One could theoretically use a different single IM for each component of a given period, yet this may unnecessarily complicate the Probabilistic Safety Assessment of the NPP systems.

Table 10a: Median limit-state IMs of fragility curves given the period of the pump.

Pump period	Lognormal fragility median (g)							
	PGA	Sa(T_1)	Sa(0.10 s)	Sa(0.15 s)	Sa(0.20 s)	AvgSa (0.1-0.4s)	AvgSa (0.1-0.2s)	AvgSa (0.05-0.15s)
0.02s	0.943	0.992	1.581	1.943	2.153	2.001	1.920	1.559
0.03s	0.814	0.900	1.364	1.676	1.858	1.726	1.656	1.344
0.04s	0.729	0.846	1.222	1.501	1.664	1.546	1.483	1.204
0.05s	0.659	0.806	1.105	1.358	1.505	1.398	1.342	1.089
0.06s	0.592	0.778	0.992	1.219	1.351	1.256	1.205	0.978
0.07s	0.540	0.755	0.904	1.111	1.232	1.144	1.098	0.892
0.08s	0.489	0.736	0.820	1.007	1.116	1.037	0.995	0.808
0.09s	0.454	0.724	0.760	0.934	1.035	0.962	0.923	0.749
0.101s	0.420	0.709	0.705	0.866	0.960	0.892	0.856	0.695
0.11s	0.384	0.686	0.644	0.792	0.878	0.815	0.783	0.635
0.12s	0.347	0.657	0.582	0.715	0.792	0.736	0.706	0.573
0.13s	0.317	0.627	0.532	0.653	0.724	0.673	0.646	0.524
0.14s	0.283	0.569	0.474	0.582	0.645	0.600	0.575	0.467
0.15s	0.244	0.502	0.408	0.502	0.556	0.517	0.496	0.403
0.16s	0.210	0.445	0.351	0.432	0.479	0.445	0.427	0.346
0.17s	0.181	0.394	0.303	0.372	0.412	0.383	0.367	0.298
0.18s	0.158	0.352	0.264	0.325	0.360	0.335	0.321	0.261
0.19s	0.139	0.315	0.232	0.285	0.316	0.294	0.282	0.229
0.20s	0.125	0.284	0.209	0.257	0.284	0.264	0.254	0.206
0.22s	0.105	0.235	0.175	0.215	0.239	0.222	0.213	0.173
0.24s	0.088	0.198	0.147	0.181	0.201	0.186	0.179	0.145
0.26s	0.076	0.169	0.127	0.156	0.173	0.160	0.154	0.125
0.28s	0.066	0.146	0.111	0.136	0.151	0.140	0.135	0.109
0.30s	0.059	0.127	0.099	0.121	0.134	0.125	0.120	0.097
0.32s	0.051	0.112	0.086	0.106	0.117	0.109	0.104	0.085
0.34s	0.046	0.099	0.077	0.095	0.105	0.098	0.094	0.076
0.36s	0.042	0.089	0.070	0.086	0.096	0.089	0.085	0.069
0.38s	0.038	0.080	0.064	0.079	0.087	0.081	0.078	0.063
0.40s	0.035	0.072	0.059	0.073	0.081	0.075	0.072	0.058
0.45s	0.030	0.057	0.050	0.062	0.068	0.064	0.061	0.050
0.50s	0.025	0.046	0.043	0.052	0.058	0.054	0.052	0.042
0.55s	0.022	0.038	0.037	0.046	0.051	0.047	0.045	0.037
0.60s	0.020	0.032	0.033	0.041	0.045	0.042	0.040	0.033
0.65s	0.018	0.027	0.030	0.037	0.041	0.038	0.037	0.030
0.70s	0.017	0.024	0.028	0.035	0.039	0.036	0.035	0.028
0.75s	0.016	0.021	0.027	0.033	0.037	0.034	0.033	0.027
0.80s	0.015	0.018	0.026	0.031	0.035	0.032	0.031	0.025
0.85s	0.014	0.016	0.024	0.029	0.033	0.030	0.029	0.024
0.90s	0.013	0.014	0.023	0.028	0.031	0.029	0.027	0.022
0.95s	0.013	0.013	0.022	0.027	0.030	0.027	0.026	0.021
1.00s	0.012	0.012	0.021	0.026	0.028	0.026	0.025	0.021

Table 10b: Dispersions of limit-state IMs given the period of the pump. Bold type is used to indicate the most efficient choice excluding the case of Sa(T_1).

Pump period	Lognormal fragility dispersion							
	PGA	Sa(T_1)	Sa(0.10s)	Sa(0.15s)	Sa(0.20s)	AvgSa (0.1-0.4s)	AvgSa (0.1-0.2s)	AvgSa (0.05-0.15s)
0.02s	**0.425**	0.417	0.494	0.495	0.505	0.467	0.483	0.468
0.03s	**0.165**	0.132	0.282	0.294	0.327	0.251	0.275	0.235
0.04s	**0.157**	0.119	0.246	0.276	0.310	0.246	0.248	0.201
0.05s	**0.186**	0.102	0.241	0.273	0.327	0.268	0.249	0.189
0.06s	0.213	0.106	0.214	0.267	0.338	0.277	0.242	**0.168**
0.07s	0.246	0.113	0.204	0.270	0.347	0.296	0.245	**0.165**
0.08s	0.263	0.126	0.186	0.255	0.326	0.291	0.231	**0.167**
0.09s	0.274	0.122	0.155	0.239	0.320	0.291	0.211	**0.152**
0.101s	0.304	0.147	**0.147**	0.228	0.327	0.304	0.210	0.172
0.11s	0.306	0.133	0.167	0.207	0.311	0.294	0.188	**0.160**
0.12s	0.323	0.151	0.223	0.213	0.330	0.323	0.208	**0.200**
0.13s	0.303	0.093	0.212	0.160	0.285	0.293	**0.156**	0.158
0.14s	0.291	0.057	0.208	**0.116**	0.257	0.269	0.128	0.152
0.15s	0.272	0.047	0.186	**0.047**	0.227	0.243	0.089	0.143
0.16s	0.262	0.016	0.203	0.099	0.208	0.229	**0.092**	0.166
0.17s	0.262	0.009	0.223	0.154	0.176	0.219	**0.112**	0.196
0.18s	0.259	0.005	0.240	0.173	0.134	0.215	**0.123**	0.216
0.19s	0.261	0.004	0.263	0.201	**0.078**	0.210	0.150	0.242
0.20s	0.261	0.004	0.285	0.225	**0.004**	0.197	0.176	0.263
0.22s	0.245	0.004	0.306	0.261	**0.141**	0.154	0.222	0.285
0.24s	0.244	0.004	0.329	0.296	0.214	**0.150**	0.264	0.311
0.26s	0.247	0.004	0.364	0.332	0.254	**0.143**	0.302	0.342
0.28s	0.260	0.003	0.390	0.363	0.295	**0.165**	0.337	0.368
0.30s	0.260	0.002	0.406	0.385	0.326	**0.176**	0.361	0.384
0.32s	0.265	0.002	0.417	0.403	0.348	**0.187**	0.379	0.396
0.34s	0.293	0.002	0.450	0.434	0.379	**0.215**	0.409	0.426
0.36s	0.314	0.002	0.473	0.455	0.401	**0.242**	0.432	0.446
0.38s	0.331	0.002	0.499	0.473	0.420	**0.269**	0.452	0.468
0.40s	0.342	0.002	0.516	0.491	0.441	**0.291**	0.471	0.484
0.45s	0.377	0.002	0.552	0.524	0.482	**0.346**	0.508	0.523
0.50s	0.409	0.002	0.582	0.566	0.524	**0.395**	0.547	0.558
0.55s	0.436	0.001	0.605	0.587	0.550	**0.429**	0.570	0.581
0.60s	**0.459**	0.001	0.631	0.620	0.582	0.462	0.600	0.607
0.65s	**0.466**	0.001	0.643	0.636	0.590	0.473	0.614	0.621
0.70s	**0.469**	0.001	0.645	0.638	0.594	0.481	0.618	0.623
0.75s	**0.471**	0.001	0.642	0.636	0.603	0.487	0.619	0.620
0.80s	**0.494**	0.001	0.661	0.657	0.627	0.510	0.641	0.640
0.85s	**0.533**	0.001	0.692	0.691	0.658	0.545	0.674	0.674
0.90s	**0.560**	0.001	0.721	0.723	0.688	0.576	0.705	0.705
0.95s	**0.570**	0.001	0.731	0.732	0.701	0.590	0.715	0.714
1.00s	**0.581**	0.001	0.740	0.740	0.714	0.603	0.725	0.723

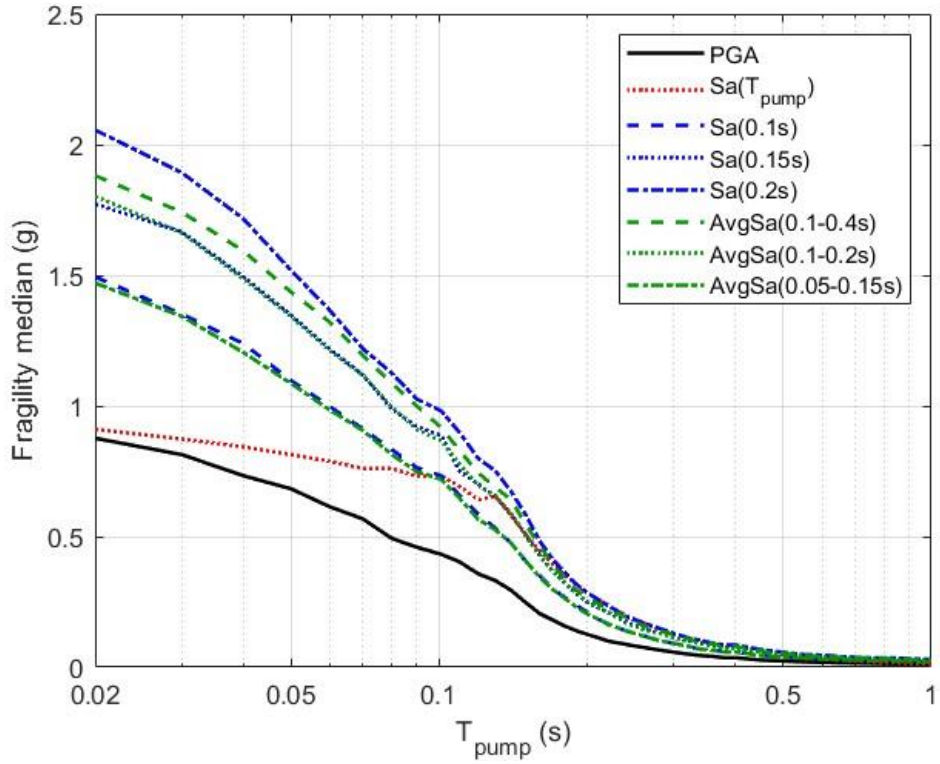

Figure 8: Median limit-state IMs of fragility curves given the period of the pump.

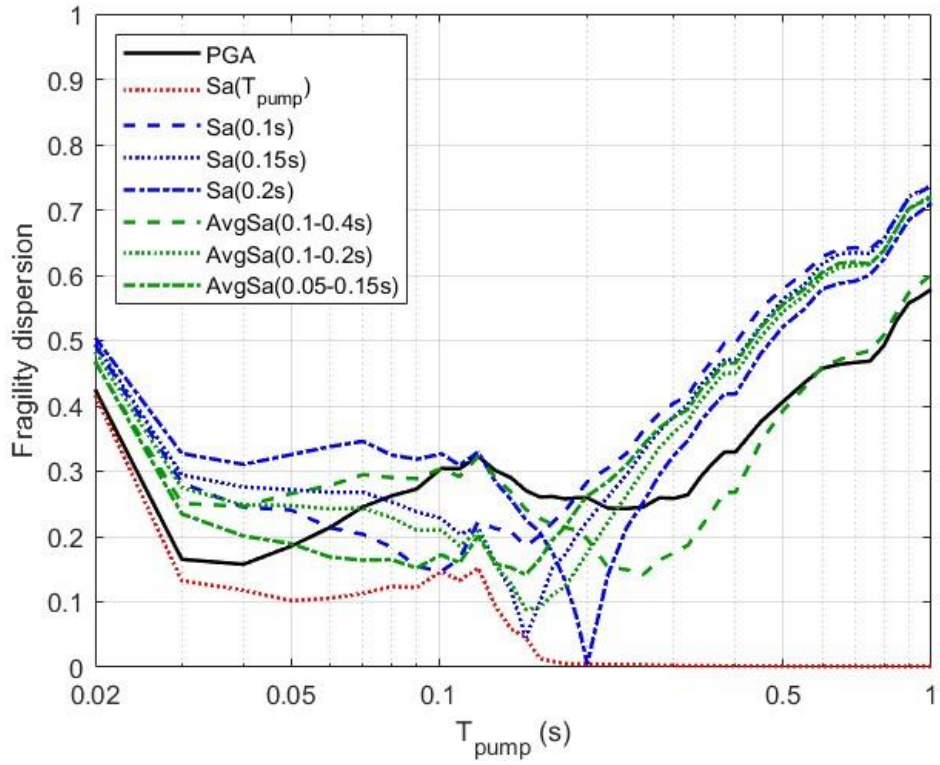

Figure 9: Dispersions of limit-state IMs given the IM and the period of the pump.

To better summarize the previous findings, we examined five distinct scenarios, assigning different weighting factors to different periods in order to account for the relative importance of the components having periods within each range. The resulting factors are outlined in Table 11. In the first scenario, all components are assigned equal weighting factors. In the other scenarios, components are categorized into separate groups, and each component within a group is assigned a weighting factor. Each weighting factor is equal to the associated value divided by the number of components in each group; in all cases, the sum of the sub-group weights adds up to one. In scenarios 2 to 5, the approach is to allocate greater weight to components with shorter to medium periods, as opposed to those with periods close to 1.00 s. Table 12 shows the weighted dispersion results, where the optimal option (i.e., lowest value) is determined is indicated in bold.

In retrospect, if one is prepared to offer hazard results (preferably properly cross-correlated) at every component period of interest, using a vector of Sa(T) values as the IM would be optimal, regardless of the relative importance of individual periods or components. Clearly, this procedure is too complex. On the other hand, if a single IM is sought for all different components, some version of AvgSa would consistently be the most effective option. Nevertheless, even if one decides to undertake the cost of upgrading fragility functions to a different IM than PGA, the selection of the appropriate range of eigenperiods to be used remains a significant consideration.

Table 11: Weighting factor given the case study and the period range.

Scenario 1		Scenario 2		Scenario 3		Scenario 4		Scenario 5	
Period range	Weight	Period range	Weight	Period range	Weight	Period range	Weight	Period range	Weight
0.02–1.00s	1.00	0.02–0.10 s	0.60	0.02-0.14 s	0.35	0.02 - 0.11 s	0.40	0.02 - 0.05 s	0.20
								0.06 - 0.15 s	0.40
		0.11–1.00 s	0.40	0.15-0.34 s	0.50	0.12 - 0.22 s	0.35	0.16 – 0.24 s	0.25
				0.36-1.00 s	0.15	0.24 - 0.50 s	0.15	0.26 – 0.40 s	0.10
						0.55 – 1.00 s	0.10	0.45 – 1.00 s	0.05

Table 12: Weighted limit-state IMs dispersions per weighting scenario and IM type. Bold type is used to indicate the most efficient choice excluding the case of Sa(T_1).

Intensity Measure	Scenario 1	Scenario 2	Scenario 3	Scenario 4	Scenario 5
	Weighted Dispersion				
PGA	0.33	**0.29**	0.29	0.29	0.28
Sa(T_1)	0.05	0.10	0.05	0.07	0.08
Sa(0.10 s)	0.40	0.32	0.33	0.31	0.28
Sa(0.15 s)	0.39	0.34	0.31	0.30	0.27
Sa(0.20 s)	0.38	0.37	0.31	0.32	0.30
AvgSa(0.10-0.40 s)	**0.32**	0.31	**0.27**	**0.28**	0.27
AvgSa(0.10-0.20 s)	0.37	0.32	0.29	**0.28**	**0.25**
AvgSa(0.05-0.15 s)	0.37	0.30	0.30	**0.28**	**0.25**

4. CASE STUDY 2: Investigating the effect of hazard consistency on IM optimality assessment

In this section, we investigate the effect that ground motion hazard consistency has on the IM optimality assessment. By optimal IM here we mean the one for which the derived fragility curve has the lowest dispersion. We calculate the fragility and response hazard curves (i.e. the demand hazard) of the water pump in the reactor building located at the METIS case study site. We repeat this exercise using two approaches: (a) Multiple Stripe Analysis (MSA) and Conditional Spectrum (CS), incorporating hazard-consistent sets of records, and (b) IDA, where hazard consistency is not enforced. A comprehensive overview of the hazard-consistent record selection methodology can be found in Deliverable D5.1 (Methodology for site-specific rock-hazard-consistent record selection for mainshock-only seismicity).

We first perform PSHA calculations using METIS case study PSHA developed in OpenQuake software (Pagani et al., 2014). Information on this model can be found in Deliverable D4.6 (Application to METIS study case). This model uses a logic tree with five branching sets, each one with three branches, resulting in a total of 125 different paths. We employ two ground motion models (GMMs), each with equal weights of 0.5: one from (Kotha et al., 2020) adapted by (Weatherill, Kotha and Cotton, 2020), and the other from (Lanzano et al., 2022). In Figure 10, we show the site mean hazard curves for three IMs: Peak Ground Acceleration (PGA), Sa(0.1 s) and AvgSa within a range of oscillator periods (0.1 s-0.4 s). The spectral ordinate of Sa(0.1 s) is considered in PSHA for reasons that will be discussed later.

Table 14 shows the mean magnitude (M) and distance (R) scenarios according to the disaggregation for different IMs and return periods. The component under investigation is the same water pump that was described in Section 3 of this Deliverable. The onset of failure of the component is based on ultimate displacement criteria set at the thresholds of d_c=2.9 mm.

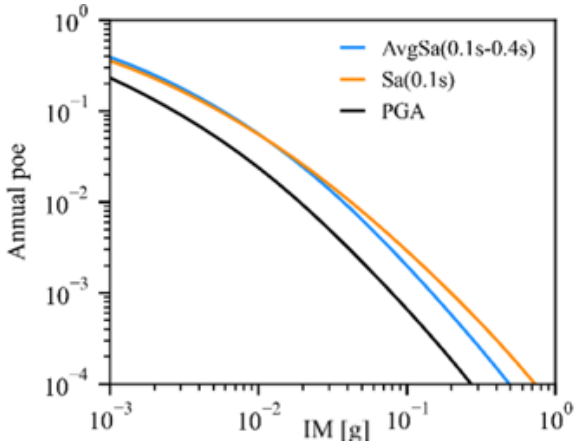

Figure 10: Hazard curves for three IMs computed for the considered rock site.

Table 13: Mean magnitude and distance (M/R in km) scenarios based on hazard disaggregation.

Return Period (yrs)	40	475	5 000	10 000	100 000
PGA	5.4/65	5.2/25	5.3/12	5.4/10	5.6/7
Sa(0.1 s)	5.2/57	5.1/22	5.2/11	5.3/10	5.3/9
AvgSa (0.1 s-0.4 s)	5.3/59	5.3/24	5.4/13	5.5/11	5.6/8

Within the framework of CS-MSA, we selected a suite of 30 records for each of ten intensity levels (IMLs) corresponding to return periods ranging from 40 to 100 000 years. We consider three conditioning IMs, namely Sa(0.01 s), AvgSa(0.1 s-0.4 s) and Sa(T_1), where T_1 is 0.1 s. For all practical purposes it is reasonable to regard Sa(0.01 s) as being numerically equivalent to PGA, a commonly

utilized IM in the nuclear industry (Zentner *et al.*, 2011). We utilized Sa(0.01s) because it is the shortest oscillator period included in the Spectral accelerations' correlation matrix established by Baker and Jayaram (2008), which is needed to create the CS. We have focused exclusively on ground motions characterized by a minimum Vs30 value of 400 m/s. Target CS is derived using the OpenQuake software and orientation-independent measure, specifically, GMRotD50 (Boore, 2010) to maintain full consistency with the GMMs adopted in the hazard computations. The sets of selected records and a more detailed description of the record selection methodology can be found in Deliverables D5.4 (Ensembles of hazard-consistent surface ground motions for mainshock seismicity) and D5.1 (Methodology for site-specific rock-hazard-consistent record selection for mainshock-only seismicity), respectively.

In the context of IDA, we employed a suite of 30 ground motion record pairs characterized as 'ordinary'—meaning they exhibit neither long-duration nor pulse-like characteristics. These records extracted from the NGA-West2 database were selected to be consistent with the hazard of a site in Greece, for the return period of 475 years (Bakalis, Kohrangi and Vamvatsikos, 2018). These records were scaled to the same intensity levels considered in the case of CS-MSA for the Italian rock site. Therefore, both sets of records, the one used in MSA and the one used in IDA, at each IML are fully consistent only in terms of the value of the conditioning IM but they do differ elsewhere in spectral content. Figures 11 and 12 show the mean and dispersion, respectively, of the spectral ordinates of the records selected for the IML corresponding to the return period of 2500 years. One can see from Figure 2 that the mean spectrum obtained with the two methods differs substantially, with the IDA-based spectrum being higher for periods longer than 0.2 s and 0.3 s for the Sa(0.01 s) and the AvgSa conditioning case, respectively, and lower otherwise. For the Sa(0.1 s) conditioning case, the IDA-based spectrum is larger for all oscillator periods with the exception of the conditioning IM where the ordinates of the two spectra coincide, of course. Additionally, in the case of CS selection, the dispersion is higher across the entire period range (Figure 3).

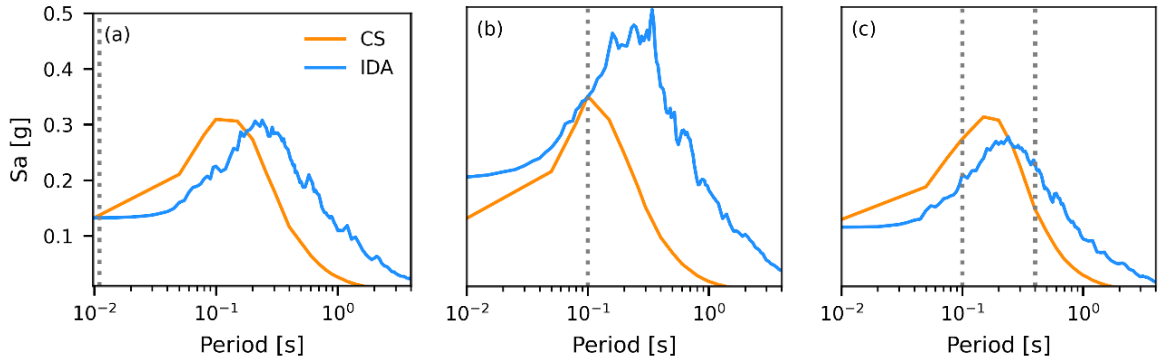

Figure 11: Mean spectra of the set of GMs selected using the CS approach and IDA approach conditioned on: (a) Sa(0.01 s), (b) Sa(0.1 s) and (c) AvgSa(0.1-0.4 s). All figures refer to the IML of 2500 years. The vertical dotted lines identify the conditioning period (in cases a and b) and the range of the AvgSa conditioning IM (case c).

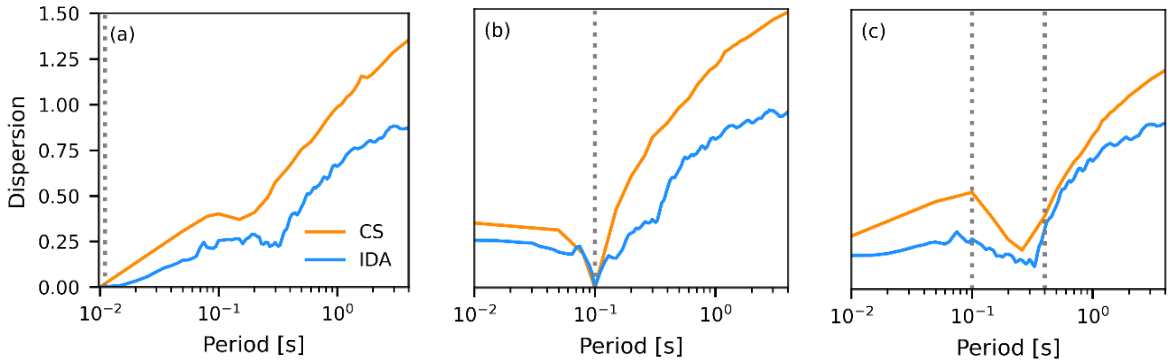

Figure 12: Dispersion of the set of GMs selected using the CS approach and IDA approach conditioned on: (a) Sa(0.01s), (b) Sa(0.1s) and (c) AvgSa(0.1-0.4s). All figures refer to the IML of 2500 years. The dotted lines have the same meaning as in Figure 2.

To derive the collapse fragility curves we fit a lognormal distribution to the structural demand values imposed by the fraction of ground motions leading to water pump failure. We estimate the mean and dispersion of the fragility curve using the method of moments for IDA and the maximum likelihood estimator for CS-MSA. In Figure 13, we present the resulting fragility curves considering all conditioning IMs and both analysis methods. It is important to highlight that the IDA fragility curves coincide with the ones derived in Section 3, as expected. Figure 14 displays the median and coefficient of variation (COV) of the pump's capacity, for the considered cases. One can see that there is a significant difference when comparing the fragility curves obtained through IDA and CS-MSA. This discrepancy underscores the critical importance of selecting ground motions that ensure site-hazard consistency. Furthermore, one can see that Sa(T_1) seems like the optimal choice for the conditioning IM, yielding the lowest dispersion in the capacity (i.e., steepest curves). However, in practical applications where the performance of multiple components with different conditioning periods located in the same building needs probabilistic assessment, the AvgSa may prove to be a good choice overall. The AvgSa-based ground motions generate fragility curves with a lower COV compared to the commonly used PGA (here replaced by Sa(0.01 s)).

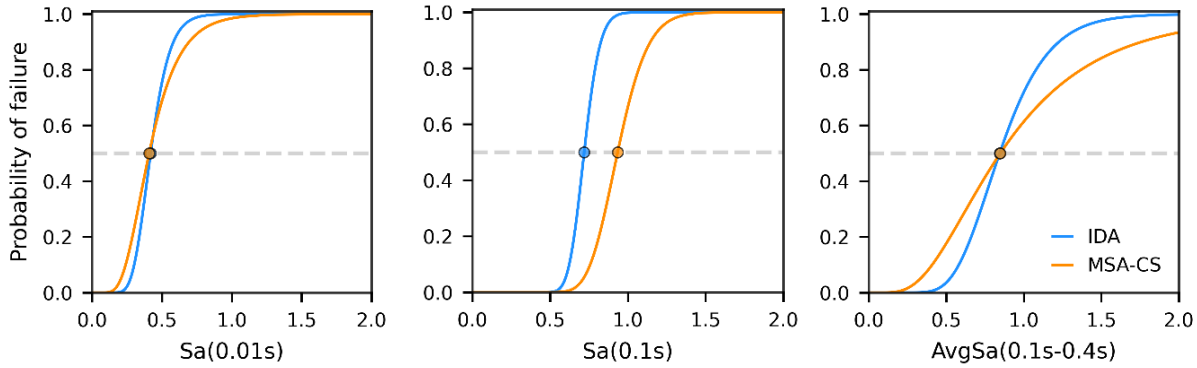

Figure 13: Fragility curves obtained using CS-MSA (orange lines) and IDA (blue lines) with different IMs. The dashed grey lines indicates the median.

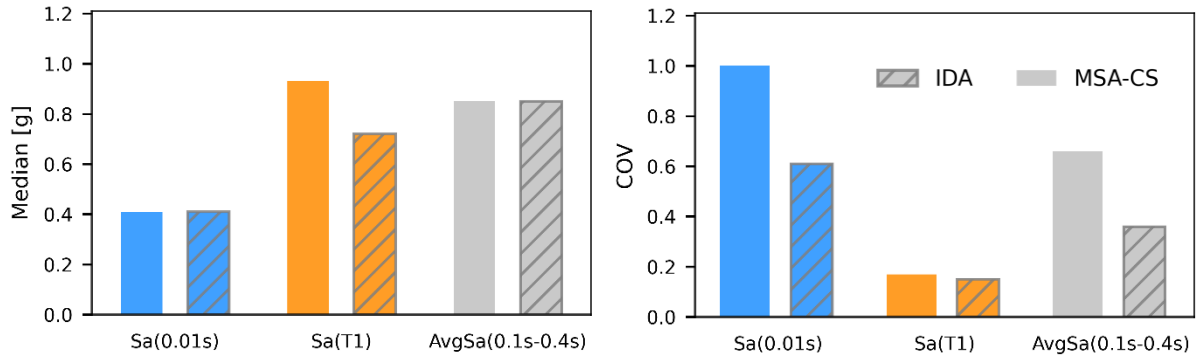

Figure 14: Median and COV of the pump capacity. Hatched bars refer to results obtained with IDA while solid ones refer to CS-MSA.

To quantify the seismic performance of the considered models, we compute the seismic response curves, which represent the annual rate of exceeding different EDP levels (the EDP considered here is the maximum displacement). These curves are derived by combining the probability of exceeding a specific demand level *EDP=edp* due to the ground motion intensity *P(EDP>edp|IM=im)* with the annual rate of 'equaling' ground motion intensity *IM* (*im*). Following the approach of Shome and Cornell (1999) *P(EDP>edp|IM=im)* can be separated into mutually exclusive collapse and non-collapse cases, resulting in the following expression:

$$\lambda_{EDP}(edp) = \int_0^{+\infty} [P(EDP > edp|\bar{C}, IM = im)(1 - P_{col}) + P_{col}]|d\lambda_{IM}(im)| \quad (8)$$

Here, $\lambda_{IM}(im)$ represents the annual rate of exceeding a given IM value *im*, P_{col} is the probability of collapse, as previously explained, and *P(EDP>edp|$\bar{C}$, IM=im)* is the probability of exceeding EDP value *edp* for a given IM value *im*, given that the component did not collapse. The distribution of non-collapse responses is modeled using a lognormal distribution with the mean and standard deviation determined via the method of moments. In Figure 15a we show the resulting response hazard curves, obtained with CS-MSA and different conditioning IMs. One can see that there is minimal difference between these curves, suggesting that all considered IMs perform similarly. However, it's important to note that the choice of the most optimal IM may become more critical when fewer IMLs and ground motions per IML are considered. Conversely, the right panel of the same figure displays response curves derived from IDA and compares them with the curve (black dotted line) calculated using CS(Sa(T_1))-MSA, which for the sake of discussion we consider the benchmark given that the variability in the capacity was slightly lower. We observe more pronounced differences between the rates of exceedance obtained using the various conditioning IMs compared to what we observed in the CS-MSA case. Additionally, even with the most optimal conditional IM (Sa(T_1)), discrepancies with the benchmark are evident. In this particular case it is interesting to note that the response hazard curve using a PGA-based IDA approach delivers unconservative estimates of the probabilities of exceeding essentially all values of the EDP. This is due to the lower dispersion of the capacity (Figure 14b) generated by the random choice of hazard-inconsistent ground motions. The response curve obtained with AvgSa approximates the benchmark results the best.

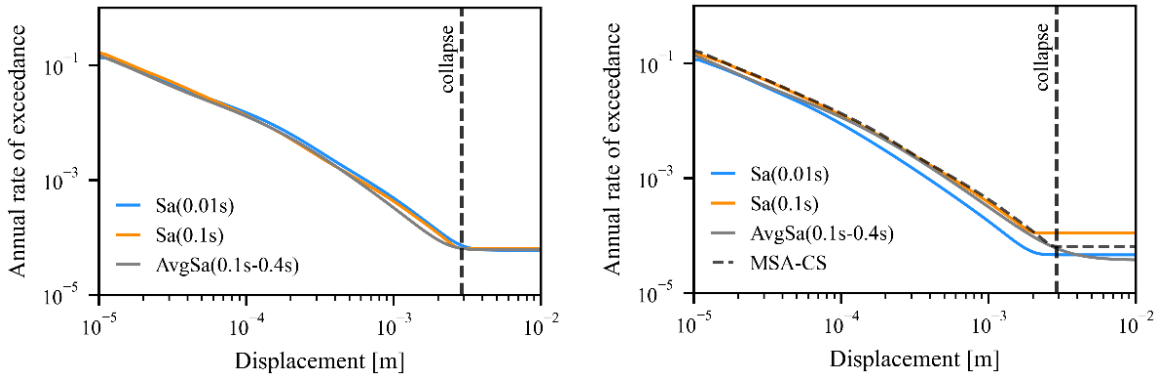

Figure 15: Response hazard curves using the CS-MSA method and different conditioning IMs (a) and using the IDA method and different conditioning IMs (b). Results are compared with the curve obtained using the CS-MSA method and Sa(T1) as conditioning IM (dashed black line).

Our findings suggest that the optimal choice of IM remains consistent regardless of the analysis method used. Sa(T_1) consistently yields results with the lowest dispersion of the fragility curve, making it the preferred choice. However, it is important to note that when evaluating the seismic risk of multiple components with varying fundamental periods mounted on the same building, Sa(T_1) might not always be the most suitable choice for all components. In such scenarios, AvgSa may emerge as a superior alternative compared to PGA, which is commonly used in the nuclear industry. AvgSa also has the practical advantage of allowing the selection of only one batch of hazard-consistent ground motions for all the response analyses concerning the different components. Lastly, we observed significant disparities in fragility and response hazard curves obtained using IDA and CS-MSA. In this particular case, the more common approach that uses IDA supported by randomly chosen ground motions scaled on the basis of their PGA values led to unconservative results. This highlights once more the critical importance of ground motion hazard consistency in risk assessment. In the case of CS-MSA, there are no substantial differences in response curves when different IMs are employed, in contrast to IDA, where results are more sensitive to the choice of conditioning IM. Here, response hazard curves generated with AvgSa align with the benchmark response curve obtained through CS(Sa(T_1))-MSA best. Note that in practical applications where fewer IMLs are chosen and fewer ground motions per IML are utilized, larger discrepancies in the response hazard curves are also expected in the CS-MSA case.

5. CASE STUDY 3: Assessment of record selection schemes, IMs and fragility analysis methods based on METIS case study

The goal of this work is to assess the impact of the record selection scheme, the conditioning IM choice and the fragility analysis method on the risk estimates. For this purpose the set of ground motion selected according to the CS-approach developed in WP5 have been used.

Indeed, in civil engineering where more conventional buildings and infrastructure are of interest, the framework of PBEE for the evaluation of seismic risk considers lower frequency spectral accelerations (Sa's) as scalar IM for hazard, conditional record selection and fragility curves development. In contrast to the structures and components of interest in nuclear safety analysis, the response of conventional buildings is generally dominated by its first (low frequency) eigenmode which makes the CS-based record selection particularly meaningful for such structures. In the present study, we will explore the sensitivity of the fragility curves of SSC of nuclear structures to the conditioning IM and to the dynamic analysis set-up adopted to compute it.

5.1. Description of ground motion used in this study

As in section 4, we adopt the METIS PSHA study developed with OpenQuake software. In METIS project, the CS-based selection of ground motion has been implemented in WP5. The approach is described in more detail in D5.1 and D5.4. For simplicity's sake, we worked here with the selected ground motion for rock conditions. Following the strategy of METIS project, the hazard was defined on (bed)rock level, and then detailed analyses were performed to introduce the site effect as reported in D5.3. The impact of site response on the results shall be analysed in future studies. Here, we use the results of the record selection without any further modification or correction.

5.1.1. Description of METIS case study hazard

We assume the nuclear installation will be located at a site in Tuscany, Italy. We use results from METIS case study PSHA (Pagani et al., 2023) developed with the OpenQuake engine (Pagani et al., 2014) . For this particular study, we select IM*$_1$=PGA and IM*$_2$=Sa(0.25 s) of the horizontal components of the ground motion as the ground motion IMs used to predict the floor acceleration responses of the reactor building. Figure 16: Hazard curves for the two selected IM*$_1$=PGA and IM*$_2$=Sa (0.26 s) (left) and UHS for six return periods.

Figure 16 displays the hazard curves of the IMs used for this study and related uniform hazard spectra. To perform multiple stripe analysis (MSA), we use the sets of CS developed in METIS project based on the CS approach (Šipčić et al., 2023). This method accounts for hazard consistency in the horizontal spectral ordinates, as discussed in previous studies (Jayaram et al., 2011; Lin, Haselton and Baker 2013). For simplicity, the vertical component was not included in the selection procedure but the procedure might be extended to vertical spectral ordinates, as discussed by Kohrangi et al. (2023). We perform record selection for ten different IM levels (IMLs) corresponding to different return periods. Table 14 summarizes the different IML values for each conditioning IM*.

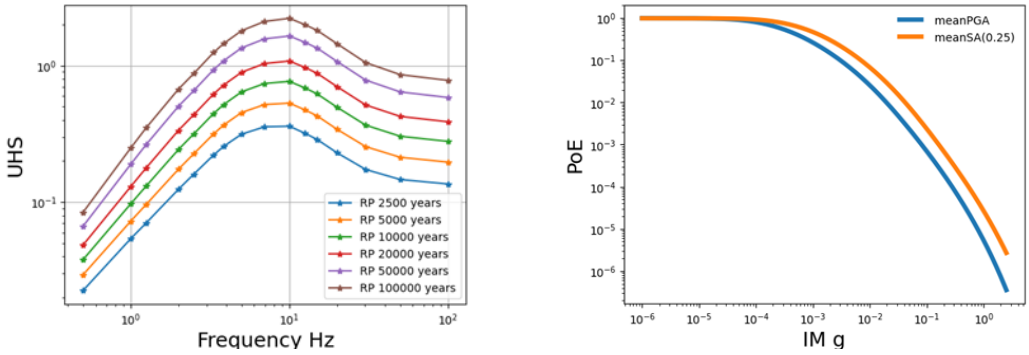

Figure 16: Hazard curves for the two selected IM*$_1$=PGA and IM*$_2$=Sa (0.26 s) (left) and UHS for six return periods.

Table 14: IML values for different return periods

IML	5	6	7	8	9	10
Return period	2500	5000	10 000	20 000	50 000	100 000
IM*$_1$=PGA (g)	0.132	0.191	0.27	0.377	0.565	0.752
IM*$_2$=Sa (0.25s) (g)	0.257	0.368	0.519	0.721	1.08	1.44

5.1.2. Analysis of ground motion time histories selected for METIS case study

In METIS project, hazard-consistent ground motion time histories have been selected in WP5 based on the conditional spectrum (CS) approach proposed by Jayaram et al. (2011) as reported in D5.1. The application to METIS case study and the development of the set of time histories used here is described with more detail in D5.4.

The target CMS and ±2σ intervals are shown in Figure 17 below for the two conditioning IMs, PGA and Sa(0.26 s) and for the 10 return periods considered for record selection. Here, we retain 5 of these return periods: IML_5, IML_6, IML_7, IML_8, IML_9, corresponding to 2500, 5000, 10 000, 25 000, 50 000 years.

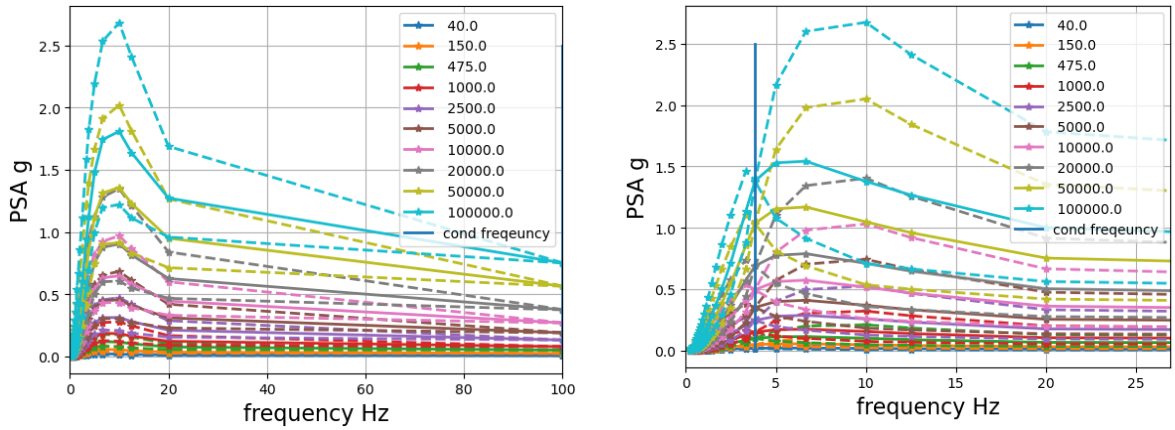

(a) PGA **(b) Sa(0.26 s)**

Figure 17: Target median and ±2σ spectra defined for record selection in WP5.

5.2. Scaling factors as low as 0.2 and as high as 10 were applied. Description of the reactor building model and fragility analysis methods

5.2.1. Structural model of reactor building

The reactor building consists of a containment and an outbuilding located on a common foundation. The sealed cylindrical shell with an inner diameter of 45.0 m is located centrally, symmetrically in the outbuilding, measuring 66.0 x 66.0 meters. A reinforced concrete foundation slab of 2.4 meters in thickness is located under the reactor compartment.

The 3D view of the structural model built in Salome-meca (Delmas and Assire, 2009) and Code-Aster (Code-Aster, 2015) is illustrated in Figure 19. The model was created in the framework of the METIS project and, herein, we use this model as a case study. It is comprised of a mesh of triangular finite elements (FE) that uses 2D linear interconnected shell elements (Figure 19: Geometry of different parts

of the FE model.). The model consists of 2800 nodes, with a maximum distance of 7 meters from one another.

The results of the modal analysis are presented in Table 15. The first mode in the X direction has a frequency of 4.05 Hz and an effective mass participation of 44 %, while the first mode in the Y direction has a frequency of 3.9 Hz and an effective participation mass of 40 %. The first vertical mode has a frequency of 8.6 Hz and corresponds to the vertical vibration of the dome. Figure 20: Mode shapes visualized in Salome-meca; 1st mode Y-direction (left) and 1st mode in X-direction (right).

displays the first two mode shapes in X and Y directions.

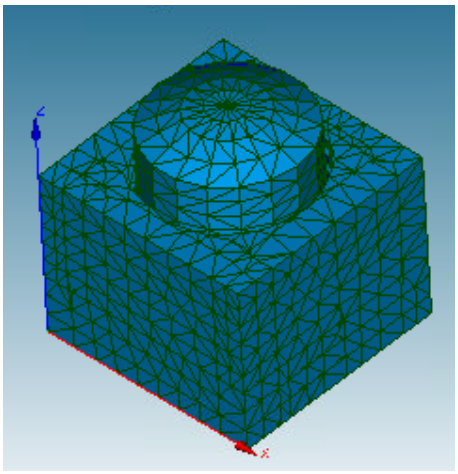

Figure 18: Finite element model mesh visualization.

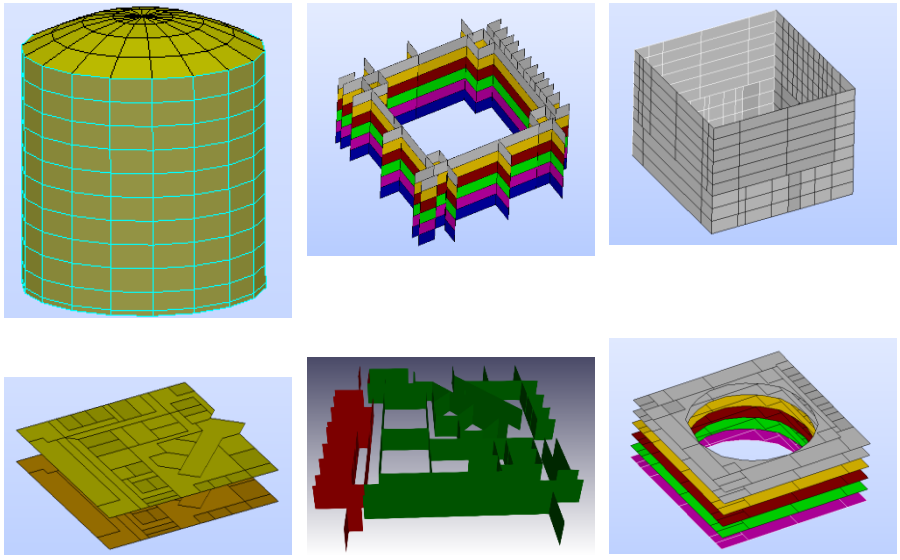

Figure 19: Geometry of different parts of the FE model.

Table 15: Modal analysis results

# of mode	Fr. (Hz)	Effective mass participation (X)	Effective mass participation (Y)	Effective mass participation (Z)
1	3.89	8.17e-02	5.08e-01	2.24e-04
2	4.05	4.43e-01	8.38e-02	3.86e-08
…	…	…	…	…

7	8.61	2.50e-05	1.67e-03	1.24e-01

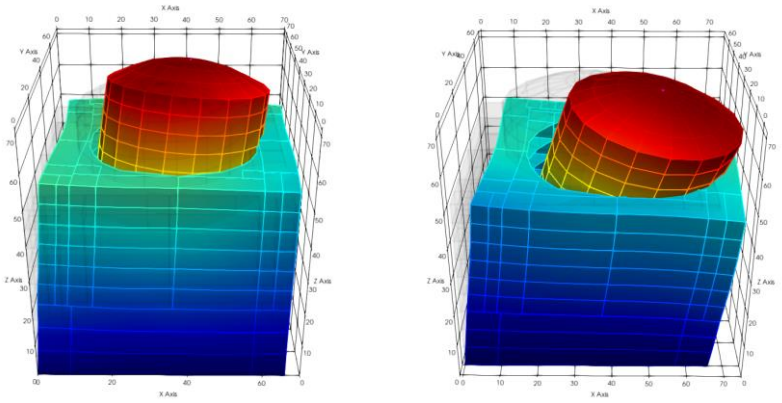

Figure 20: Mode shapes visualized in Salome-meca; 1st mode Y-direction (left) and 1st mode in X-direction (right).

Note that a few modelling simplifications have been adopted: the tendons of the dome, the cylindrical part and the nuclear reactor's internal parts, including walls and floors, have not yet been included in the model. These shortcomings might influence the floor acceleration response at several locations compared to the response of the actual structure. However, the purpose of this study was to test how different sets of records selected according to different IMs affect the response of SSCs mounted in the reactor building. This goal is not obstructed by an approximate estimation of the floor accelerations.

The structural response of the reactor building was computed accounting for soil-structure interaction. In this framework, the ground is accounted for by complex frequency dependent impedance matrices.

In particular, we assess the model through the computation of transfer functions (white noise input) and we compute structural response analysis.

For each run, we monitor EDPs, including the maximum peak floor acceleration and the floor spectral acceleration for a wide range of frequencies in all three directions and at four selected levels (1st level at 6 meters, 2nd level at 12 meters, 3rd level at 37 meters and 4th level at 64 meters-dome) in the base part of the reactor locations (see Figure 26).

We then investigate:

- the sensitivity of both fragility curve's parameters, $\widehat{A_m}$ and β_R, to the IM* of the rock ground motions,
- the sensitivity to the record selection and fragility estimation analysis set-up, namely MSA and Cloud Analysis (a.k.a. regression).

The results are reported in Section 5.3.

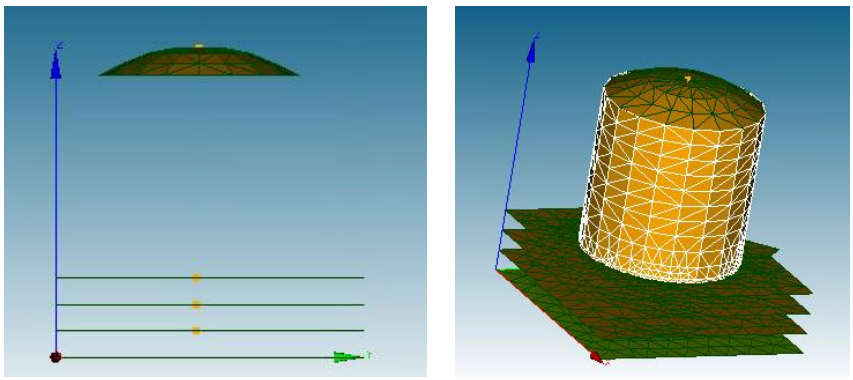

Figure 21: Post-processing points of the structural model.

5.2.2. Approaches for the development of hazard-consistent fragility curves

There are different ways to derive fragility curves, but here we consider only MSA and cloud analysis (Zentner, Gündel and Bonfils, 2016). We derive fragility curves based on MSA outputs presented in the previous section, and we also use the IM-EDP pairs of MSA to perform cloud analysis.

We first explain the procedure with MSA. We estimate the probability that the EDP exceeds the capacity threshold at each stripe. We can calculate Probabilities of Exceedance (PoEs) by counting the exceedances of the specific EDP at each stripe or by fitting a lognormal model at each stripe. The final step is to fit a lognormal model to the PoEs' Empirical Cumulative Density Function (ECDF).

The alternative way is to use the IM-EDP pairs coming from MSA and perform cloud analysis. Under the assumption that the IM-EDP relationship is lognormal, we fit a linear regression model in the lognormal space to establish a relationship between IM-EDP. We estimate the standard error of estimation and use it as the conditional dispersion along the regression line. We then evaluate the PoEs for different points across the regression line and fit a lognormal curve (Zentner, Gündel and Bonfils, 2016).

For the MSA, the IM used for evaluating the fragility curves must be the same as the conditioning IM* utilized in record selection. This is not the case for the regression approach. Any record selection procedure can be used. In particular, both IM* sets can be used together for the regression (provided that the two sets do not have ground motions in common, as is the case here). Consequently, the regression approach can be easily extended to the vector fragility case, which is one of the reasons why it is considered here in addition to MSA.

Seismic fragility curves for a given limit state (e.g., failure) provide the conditional probability that the engineering demand parameter (EDP, here called generically y) exceeds a threshold, y_{crit}, associated with the onset of the limit state for a given level of ground motion intensity, a:

$$P_f(a) = P(y > y_{crit}|a) \tag{9}$$

When the widely adopted lognormal fragility model proposed by (Kennedy et Al., 1980; Huang et Al. 2011: Zentner et al., 2016) is applied, the shape of the fragility curve is approximated by the cumulative distribution function of a lognormal distribution:

$$P_f(a) = \Phi\left(\frac{lna - ln\widehat{A_m}}{\beta_R}\right) \tag{10}$$

where Φ is the CDF of the standard normal distribution N~(0,1) and $\widehat{A_m}$ denotes the median capacity. The parameter β_R, which represents the uncertainty, is the log-standard deviation. of the capacity.

In this study, we derive fragility curves for the failure of an equipment located at the first level. The damage measure is the average of the maximum floor spectral accelerations of the two horizontal directions, between 5 to 9 Hz, i.e., AvgSa (5:1:9) that we adopted as the EDP to gauge the equipment performance. For the purpose of this study, we assume two reduced failure thresholds, y_{crit}-

={0.4g,0.7g}, lower than typical failure thresholds for nuclear equipment, to better illustrate some aspects of the fragility modeling procedure.

In the next two sections we will investigate the sensitivity of both $\widehat{A_m}$ and β_R to a) the IM* of the rock ground motions and b) to the analysis set-up, namely MSA and cloud (a.k.a. regression) analysis.

5.3. Results

5.3.1. Transfer function analysis

In this first subsection, we discuss the results of the TF analysis. We perform TF analysis to understand better the dynamic behavior of the reactor building and the locations at which we expect high floor acceleration demands. The TF analysis is performed in code-aster by inputting a uniform unitary frequency signal and measuring the response and amplification at different spectral frequencies at various locations. Figure 22: TF along height for different directions: X-direction (left), Y-direction (middle) and Z-direction (right).

shows the TF at different frequencies for different reactor locations-elevations (Floor 1 at 6 meters, Floor 2 at 12 meters, Reactor base at 37 meters and 4th level at 64 meters-dome) and in three different directions. We observe that the amplification is more evident at the top floors. The amplification in the vertical direction is also of high importance.

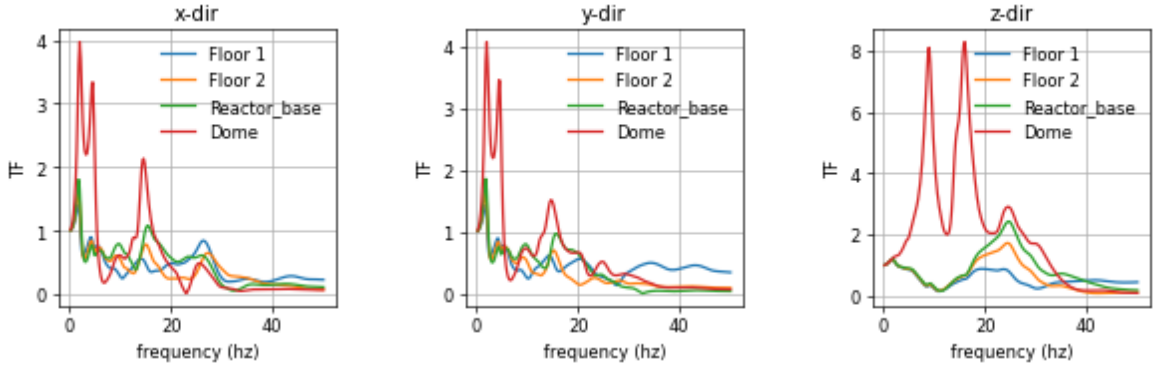

Figure 22: TF along height for different directions: X-direction (left), Y-direction (middle) and Z-direction (right).

5.3.2. Multiple stripe analysis and sensitivity of the floor acceleration response on the conditioning IM

For this study, we run the two sets of ground motions associated with the five stripes from 5 to 9 listed in Table 14, which were selected based on the CS approach with IM*$_1$=PGA and IM*$_2$=Sa(0.25s) as conditioning IMs. As an illustrative example, Figure 23: Single ground motion record plots (IML_8/Coalinga, RSN401, sequence number 401); ground motion time histories (first column); floor acceleration time histories (second column); floor acceleration response spectra (third column). The time histories in the first, second and third rows refer to x, y, and z directions, respectively. shows the ground motion time histories, the floor response acceleration time history and the floor response spectra for three different directions at the base of the building for a particular ground motion record. We observe higher spectral amplifications at frequencies between 5-10 Hz, especially in the X-direction.

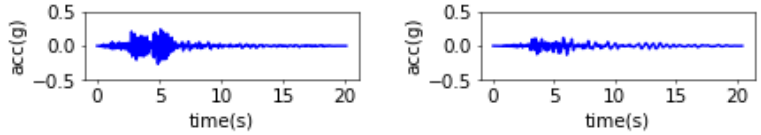

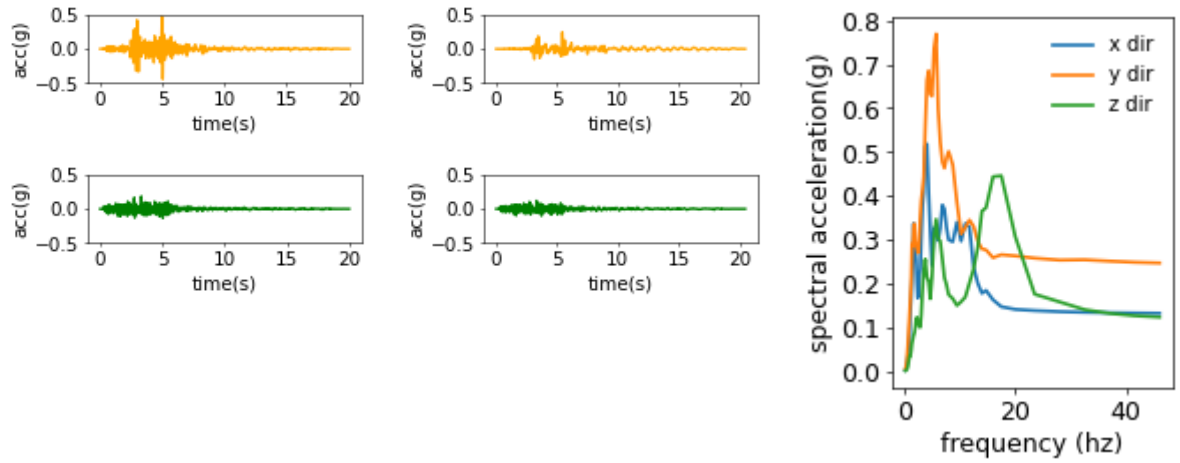

Figure 23: Single ground motion record plots (IML_8/Coalinga, RSN401, sequence number 401); ground motion time histories (first column); floor acceleration time histories (second column); floor acceleration response spectra (third column). The time histories in the first, second and third rows refer to x, y, and z directions, respectively.

Figure 24 (left) shows the median floor spectral acceleration (FSA) at 100 Hz (similar to PFA) at the dome of the building using the two sets of ground motion records. The estimates of the median PFA seem to have minor sensitivity to the choice of the conditioning IM*. However, the dispersion of the response at the dome in each one of the three directions (Figure 24: MSA-Sensitivity of the floor spectral acceleration (FSA) response to the conditioning IM; from left to right, median (left) and dispersion (middle) at 4th level-dome; dispersion at 1st level (right)., middle) is very sensitive to the selected IM*. As a matter of fact, the sensitivity of the IM* on the dispersion varies from location to location. IM^*_2 seems to better predict the floor response at the highest levels, while IM^*_1 is a better indicator for the floor responses closer to the ground (Figure 24: MSA-Sensitivity of the floor spectral acceleration (FSA) response to the conditioning IM; from left to right, median (left) and dispersion (middle) at 4th level-dome; dispersion at 1st level (right)., right).

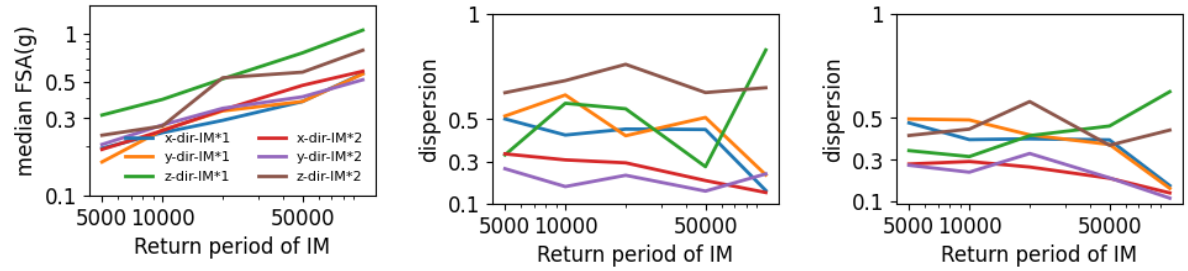

Figure 24: MSA-Sensitivity of the floor spectral acceleration (FSA) response to the conditioning IM; from left to right, median (left) and dispersion (middle) at 4th level-dome; dispersion at 1st level (right).

5.3.3. Sensitivity analysis on the conditioning IM*

First, we explore the sensitivity analysis of the conditioning IM* on SSC's fragility curves (computed via MSA). Figure 25: Fragility curves comparison for the two different conditioning IM*s ; first row: fragility curves of component at level1 with an assumed failure threshold of 0.4g; second row: fragility curves of component at level1 with assumed failure threshold of 0.7g; third row: fragility curves of component at level1 with assumed failure threshold of 0.4g based on scaled MSA-IML7 set; first column: estimation of PoEs with a lognormal model; second column: estimation of PoEs with direct estimation of exceedances

Table 16: Comparison of fragility parameters for the two conditioning IM*s (PGA and Sa(0.25s)

Intensity measure (IM*)	Fragility parameters							
	Lognormal PoEs				Direct PoEs			
	$\widehat{A_m}$		β_R		$\widehat{A_m}$		β_R	
	IM^*_1	IM^*_2	IM^*_1	IM^*_2	IM^*_1	IM^*_2	IM^*_1	IM^*_2
MSA-threshold 0.4g	0.37	0.72	0.34	0.37	0.36	0.69	0.26	0.43
MSA-threshold 0.7g	1.15	2.07	0.48	0.48	0.68	1.31	0.13	0.14
Scaled MSA-threshold 0.4g	0.34	0.66	0.26	0.28	0.34	0.66	0.19	0.31

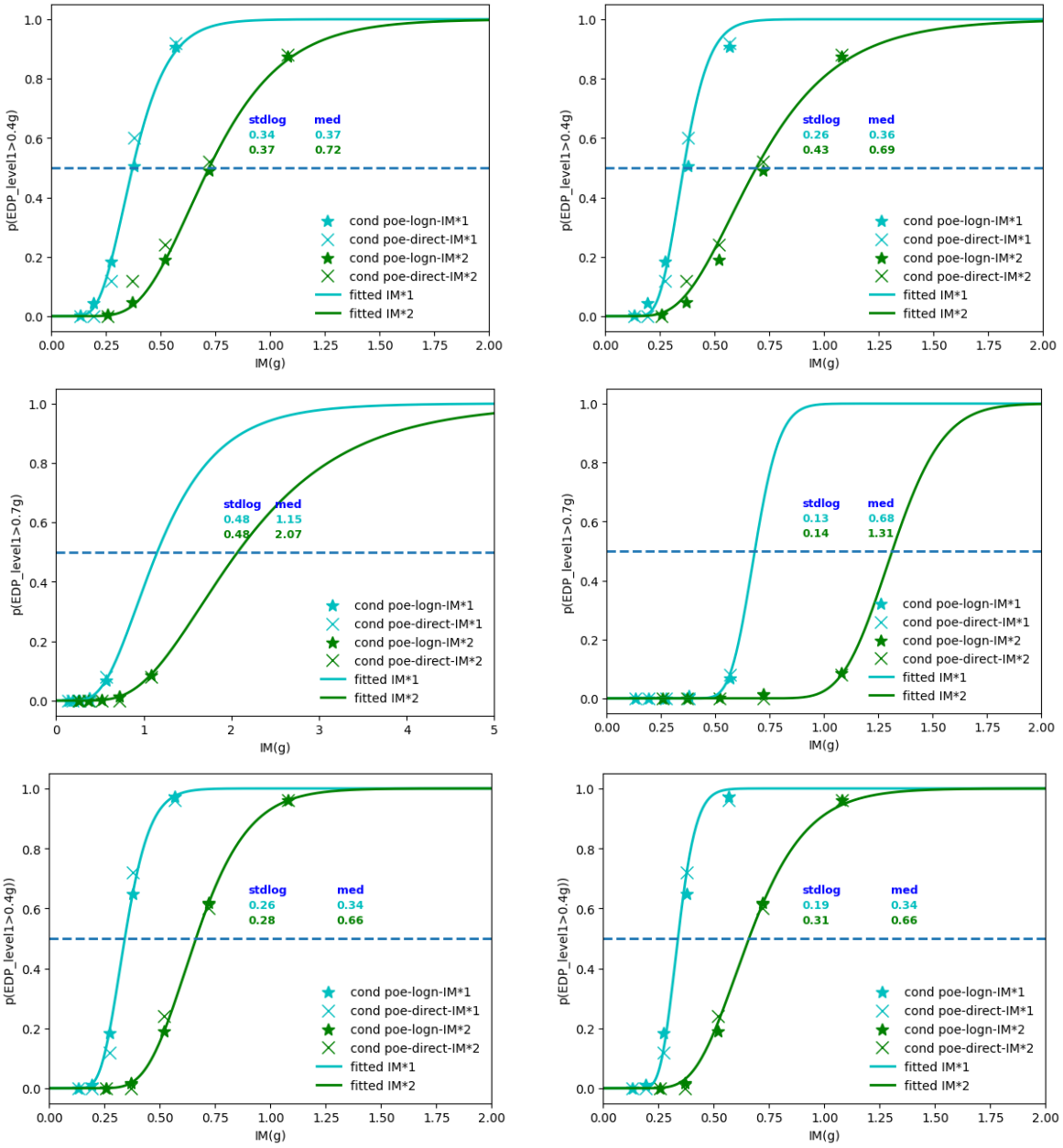

Figure 25: Fragility curves comparison for the two different conditioning IM*s ; first row: fragility curves of component at level1 with an assumed failure threshold of 0.4g; second row: fragility curves of component at level1 with assumed failure threshold of 0.7g; third row: fragility curves of component at level1 with assumed failure threshold of 0.4g based on scaled MSA-IML7 set; first column: estimation of PoEs with a lognormal model; second column: estimation of PoEs with direct estimation of exceedances

5.3.4. Sensitivity analysis on the analysis method, MSA vs Cloud analysis

The scope of this subsection is to perform a sensitivity analysis of the fragility curves to the method analysis set-up (MSA vs cloud analysis) adopted for estimating the seismic demand. As we describe in the previous section, to perform regression analysis, we need to use the IM-EDP pairs from MSA. We already have two datasets from the CS-MSA for the two different conditioning IM*s. To perform the regression analysis, we can use either the dataset from each conditioning IM* separately or merge the two different datasets.

Figure 26 displays the fitted regression lines based on the three cases, the first two for each distinct dataset of MSA, and the third one corresponds to the merged dataset. We observe that the regression outputs are somewhat insensitive to the dataset selection, indicating the robustness of the approach.

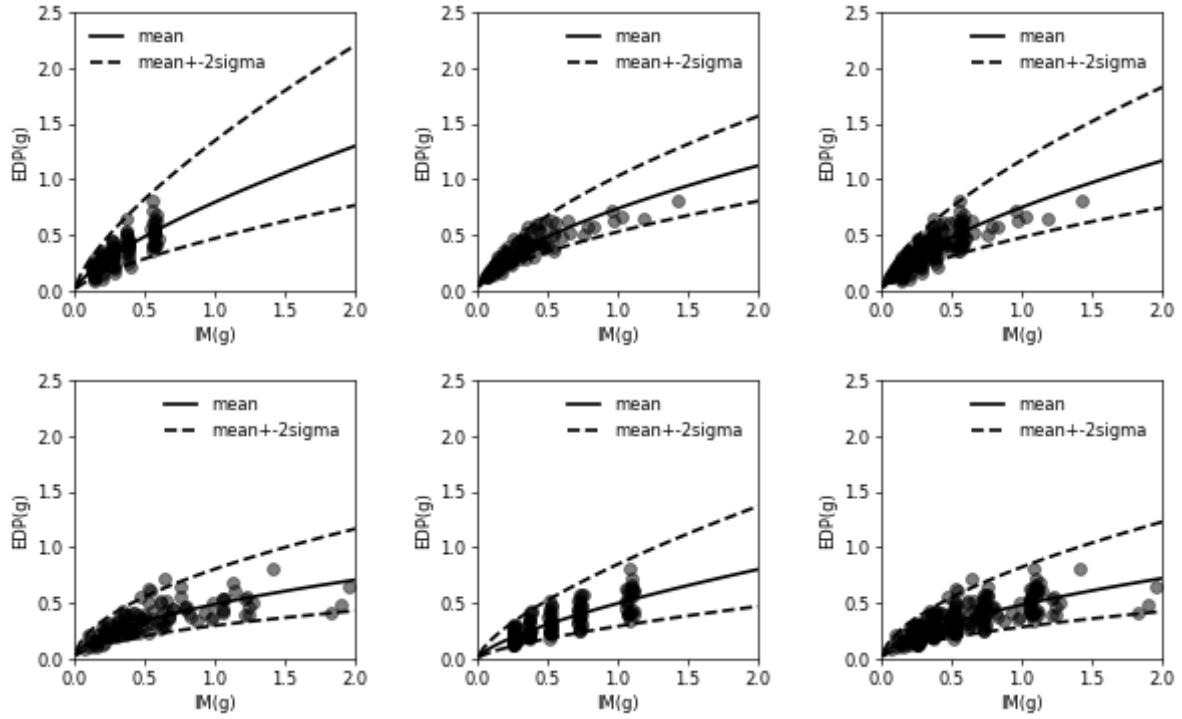

Figure 26: regression plots (IM-EDP)-sensitivity to the dataset selection; first row corresponds to IM=Sa(0.01s) for the two different datasets and the merged one; second row corresponds to IM=Sa(0.25s); from left to right, MSA-IM*=Sa(0.01s), MSA-IM*=Sa(0.25s) and merged dataset.; SSC located at 1st level with an assumed failure threshold of 0.4g;Note that the black dots indicate that there are more data concentrated around those values compared to grey dots.

The next step is to derive fragility curves based on regression analysis carried out on the cloud of data. This presupposes that we can estimate the PoEs. For that, we adopt the classical lognormal relation between the EDP and the IM (Zentner et al., 2016). Note that the standard error is constant along the regression line and doesn't change with the level of intensity in the log-space, however it does increase in physical space, as can be observed in the Figures, in agreement with the assumption of lognormal fragility curve.

The last part of this subsection compares the fragility curves based on regression analysis and MSA. We are comparing the case of IM^*_1=Sa(0.01 s) and IM^*_2=Sa (0.25 s), each for the three different datasets used. The first row of this figure corresponds to IM^*_1 and the second row to IM^*_2. We observe little differences between MSA and regression fragility curves (Figure 27). As a final check, we also use risk metrics to compare the efficiency of the different methods by integrating the fragility and the hazard curves. Table 16 compares the annual rate of exceeding this damage state (for SSC located at 1st level with an assumed failure threshold of 0.4g) for the different approaches (for the regression method, we show just the case with the merged dataset). The risk estimates differ due to the limited ground motion sample size utilized here, are minor and negligible here. This is due to the fact that the beta values from

the fragility curves were similar for the different IM and is not general result. Obviously, the convolution of the fragility and hazard curves to total failure probabilities depends both on the fragility and hazard parameters.

Additional studies conducted by the authors highlighted differences in the risk estimates that depend on the performance of the IM and thus the choice of conditioning IM.

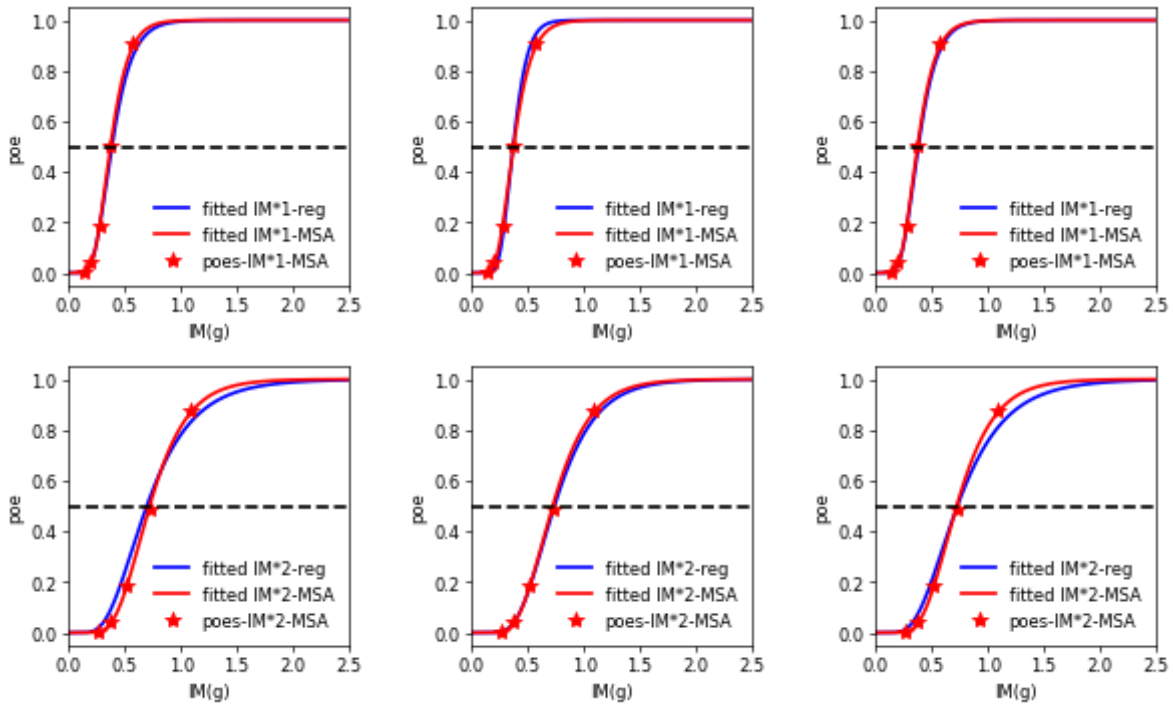

Figure 27: Comparison of fragility curves for MSA and regression analysis; comparison for IM^*_1=Sa(0.01s (top) and IM^*_2=Sa (0.25s) (bottom) for the three different datasets; from left to right, IM*=Sa(0.01s), IM*=Sa(0.25s) and the merged dataset; SSC located at 1st level with an assumed failure threshold of 0.4g;

Table 16: Annual failure probabilities for equipment located at1st level with an assumed failure threshold of 0.4g;

Intensity measure (IM*)	×1e-05	Fragility parameters	
		$\widehat{A_m}$	β_R
Sa(0.01s)-MSA	7.680	0.37	0.34
Sa(0.25s)-MSA	7.526	0.72	0.37
Sa(0.01s)-reg/merged	8.234	0.36	0.35
Sa(0.25s)-reg/merged	9.644	0.683	0.45

5.3.1. Vector IMs-discussion

One of the objectives of this study is to lay the foundations for introducing a new approach that includes vector IMs in the seismic risk analysis of nuclear power plants. As stated earlier, we reiterate here that in the framework of probabilistic seismic risk analysis (PRA) of nuclear power plants, a single ground motion intensity measure (IM) is generally used as a predictor of the performance of structures, systems, and components (SSCs) subject to earthquakes. In most cases, Peak Ground Acceleration (PGA) is the IM of choice.

Several studies (Soroushian et al. 2016; Ryan et Al 2016) have shown that there are components that are sensitive to vertical floor accelerations. In nuclear engineering practice, several SSCs are sensitive to the vertical floor acceleration demand. To better predict vertical floor acceleration demands and

reduce the variability in the fragility curves of those SSCs, a vector IM that includes both the horizontal and the vertical component of the ground motion can be used. This will be the object of further analysis conducted by the authors.

5.4. Summary and insights from this study

The use of the CS approach for record selection allows for considering scenario spectra with more realistic spectral shapes as opposed to the UHS, which is generally used as the target for record selection or simulation.

The analysis of the time histories selected according to the CS approach and their use for the computation of floor response and fragility curves allowed for a first set of recommendations for nuclear applications:

- Our findings suggest that the slope of the fragility curve is sensitive to the conditioning IM. Here, the choice of the IM had a minor impact on the total failure rates but this was not the case for other applications. Obviously, risk estimates depends on the conditional failure probabilities evaluated for the stripes and thus the fragility parameters, as well as the hazard curves, both depend on the IM ans its performance to predict hazard and structural failure. In consequience, it is not expected that the risk estimats are the same for different conditioning IMs.

- The fragility curves obtained from MSA and cloud analysis are very similar. The robustness of these results will be tested using more SSCs and different analysis set-ups.

6. Overall conclusion and recommendations

There are numerous existing IMs found in the literature and presented in Section 1, each accounting for different characteristics of ground motions. They can be categorized as either structure-specific or non-structure-specific. Currently, scalar IMs are predominantly utilized in evaluating the performance of conventional buildings and critical infrastructure, such as NPPs. Hence, they were the primary focus of our case studies.

The main advantage of the scalar IMs lies in the hazard availability. Conventional hazard curves are usually available for PGA and Sa(T). Additionally, if one was to use a vector IM, the correlation between the selected scalar IMs should be considered. Hazard curves for vector-valued IMs can be developed through Vector-valued Probabilistic Seismic Hazard Analysis (VPSHA).

The additional hazard computation mentioned is beyond the scope of this study. Therefore, the selection of the studied IMs was based on available hazard and PSHA results developed in previous WPs of the METIS project. Independent case studies compared the optimality of the most conventional IMs: PGA, Sa(T) and the AvgSa(T_1,T_2).

Firstly, it is crucial that the selection of ground motion records is hazard-consistent for specific sites, considering motions corresponding to the site's characteristics. Simplifications in the process, such as using arbitrary sets or interpolating the RotD50 parameter, should be avoided. A qualitative evaluation of selected GMRs can enhance results, eliminating any motions exhibiting non-ordinary features. Sets can be expanded by simulating additional GMRs.

Three approaches for seismic demand analysis were examined: the IDA analysis, CS-MSA and the Cloud Analysis. Significant differences were observed for IDA and CS-MSA, with the latter proving less sensitive to the conditioning IM. Fragility curves developed with CS-MSA and Cloud Analysis were similar, with Cloud Analysis demonstrating applicability to vector fragility cases.

Since the results were evaluated for individual components of the NPP reactor, the Sa(T) that accounted for the natural period of the observed components performed better than the conventionally used PGA. However, by considering the uncertainty of the estimation of the SSCs' period, Sa(T) superiority in terms of the smallest limit-state IM dispersion is not so evident anymore and PGA or SaAvg may be a reasonable choice provided that these IMs require fewer sets of ground motions. However, for very important or critical SSCs and based on controlled uncertainty of the SSCs' vibration periods, the Sa(T)

may be selected as the optimal IMs. However, in a more general case, it would be recommended to use vector-valued IMs taking into account the periods of several components if the aim was to evaluate the fragility of multiple components. Alternatively, IMs describing the characteristics of the vertical component of ground motions could be included, especially for components/equipment sensitive to vertical acceleration/velocity.

The main results and findings are summarized in Table 18. Additional studies beyond this project's scope could be developed to support the case study findings, testing proposed methodologies on a wider set of IMs and components. This could involve performing additional hazard analyses, computing curves for alternative IMs reflecting site-specific characteristics or synthetically placing the observed NPP in other locations with existing hazard curves for different IMs.

Table 17: Summarised results and conclusions of the case studies.

RESULTS		
OPTIMAL IM (FROM THE SELECTION)		
For components with 0.05 s <T< 0.55 s use AvgSa for the corresponding interval, while PGA is superior for T<0.05 s and a close contender for other values.	$Sa(T_1=0.1s)$ seemingly preforms the best, but it is component-specific. AvgSa was considered as an appropriate alternative when multiple components need to be evaluated.	Depends on the location (elevation).
CONCLUSIONS AND RECOMMENDATIONS		
Using a vector of Sa(T) values as the IM would be optimal, but it requires a different set of ground motions and hazard curves. If the cost of upgrading fragility functions to an IM different from PGA is undertaken, the selection of the appropriate range of natural periods to be used remains a significant consideration.	Using $Sa(T_1)$ resulted in the lowest dispersion of the fragility among the studied IMs. Significant differences were observed in the fragility and response hazard curves obtained using the two different approaches, i.e., the results are sensitive to the adopted approach. Ground motion hazard consistency in risk assessment plays an important role. The results are more sensitive to the IM selection when using the IDA, compared to the CS-MSA approach.	For better selection of the GMRs the GMRotD50 should be calculated instead of interpolated, visualisation of the selected GMRs and filtering the ones that do not exhibit ordinary features should be done. To avoid large scaling factors and other irregularities, some GMRs could be simulated. A vector IM including both the horizontal and the vertical GM components might result in better predictions of the vertical floor responses and thus reduce the variability in the fragility curves of components that are sensitive to both floor acceleration components. The slope of the fragility curve is sensitive to the conditioning IM, while the choice of the IM had a minor impact on the total failure rates. The fragility curves obtained from MSA and cloud analysis are very similar.

7. Acknowledgements

We would like to thank Pablo Garcia de Quevedo Iñarritu for creating the structural model of the reactor building in OpenSees. The contribution of Konstantin Goldsmith at the early stage of the study is also much appreciated.

8. Bibliography

Alembagheri, M. (2018). Investigating efficiency of Vector-Valued intensity measures in seismic demand assessment of concrete dams. *Advances in Civil Engineering*, *2018*, 1–12. https://doi.org/10.1155/2018/5675032

Alzate, Y. F. V., & Hurtado, J. E. (2021). Efficiency of intensity measures considering Near- and Far-Fault Ground motion records. *Geosciences*, *11*(6), 234. https://doi.org/10.3390/geosciences11060234

Alzate, Y. F. V., Hurtado, J. E., & Pujades, L. G. (2021). New insights into the relationship between seismic intensity measures and nonlinear structural response. *Bulletin of Earthquake Engineering*, *20*(5), 2329–2365. https://doi.org/10.1007/s10518-021-01283-x

Andrerson, J. C., & Bertero, V. V. (1987). Uncertainties in Establishing Design Earthquakes. *Journal of Structural Engineering*, *113*(8). https://doi.org/10.1061/(ASCE)0733-9445(1987)113:8(1709)

Arias, A. (1970). A measure of earthquake intensity. *Seismic Design for Nuclear Plants*, 438–483. http://ci.nii.ac.jp/naid/10003998002

ASCE. (2019). Seismic design criteria for structures, systems, and components in nuclear facilities. In *American Society of Civil Engineers eBooks*.

ATC. (1978). *ATC 3-06 report*.

Avşar, Ö., & Ozdemir, G. (2013). Response of Seismic-Isolated bridges in relation to intensity measures of ordinary and pulselike ground motions. *Journal of Bridge Engineering*, *18*(3), 250–260. https://doi.org/10.1061/(asce)be.1943-5592.0000340

Bakalis, K., Kohrangi, M., & Vamvatsikos, D. (2018). Seismic intensity measures for above-ground liquid storage tanks. *Earthquake Engineering & Structural Dynamics*, *47*(9), 1844–1863. https://doi.org/10.1002/eqe.3043

Bakalis, K., & Vamvatsikos, D. (2018). Seismic fragility functions via nonlinear response history analysis. *Journal of Structural Engineering-asce*, *144*(10). https://doi.org/10.1061/(asce)st.1943-541x.0002141

Baker, J. W. (2007). Probabilistic structural response assessment using vector-valued intensity measures. *Earthquake Engineering & Structural Dynamics*, *36*(13), 1861–1883. https://doi.org/10.1002/eqe.700

Baker, J. W., & Cornell, C. A. (2004). Choice of a vector of ground motion intensity measures for seismic demand hazard analysis. *13th World Conference on Earthquake Engineering*, *Paper No. 3384*. https://web.stanford.edu/~bakerjw/Publications/Baker%20Cornell%20(2004)%2013WCEE%20Manuscript.pdf

Baker, J. W., & Cornell, C. A. (2006). Spectral shape, epsilon and record selection. *Earthquake Engineering & Structural Dynamics*, *35*(9), 1077–1095. https://doi.org/10.1002/eqe.571

Baker, J. W., & Cornell, C. A. (2008a). Vector-valued intensity measures for pulse-like near-fault ground motions. *Engineering Structures*, *30*(4), 1048–1057. https://doi.org/10.1016/j.engstruct.2007.07.009

Baker, J. W., & Cornell, C. A. (2008b). Vector-valued Intensity Measures Incorporating Spectral Shape For Prediction of Structural Response. *Journal of Earthquake Engineering*, *12*(4), 534–554. https://doi.org/10.1080/13632460701673076

Bhanu, V., Chandramohan, R., & Sullivan, T. J. (2021). Influence of ground motion duration on the dynamic deformation capacity of reinforced concrete frame structures. *Earthquake Spectra*, *37*(4), 2622–2637. https://doi.org/10.1177/87552930211033879

Bianchini, M., Diotallevi, P. P., & Baker, J. (2009). Prediction of inelastic structural response using an average of spectral accelerations. *Proceedings of the 10th International Conference on Structural Safety and Reliability (ICOSSAR09), Osaka, Japan, 13–17 September 2009*.

Bojórquez, E., & Iervolino, I. (2011). Spectral shape proxies and nonlinear structural response. *Soil Dynamics and Earthquake Engineering*, *31*(7), 996–1008. https://doi.org/10.1016/j.soildyn.2011.03.006

Bojórquez, E., Iervolino, I., & Manfredi, G. (2008). Evaluating a new proxy for spectral shape to be used as an intensity measure. *AIP Conference Proceedings*. https://doi.org/10.1063/1.2963788

Bommer, J. J. (1999). Displacement spectra for seismic design. *Journal of Earthquake Engineering*, *3*(1), 1. https://doi.org/10.1142/s1363246999000028

Bommer, J. J., Magenes, G., Hancock, J., & Penazzo, P. (2004). The influence of Strong-Motion duration on the seismic response of masonry structures. *Bulletin of Earthquake Engineering*, *2*(1), 1–26. https://doi.org/10.1023/b:beee.0000038948.95616.bf

Boore, D. M. (2010). Orientation-Independent, Nongeometric-Mean Measures of Seismic Intensity from Two Horizontal Components of Motion. *Bulletin of the Seismological Society of America*, *100*(4), 1830–1835. https://doi.org/10.1785/0120090400

Bradley, B. (2010). A generalized conditional intensity measure approach and holistic ground-motion selection. *Earthquake Engineering & Structural Dynamics*, *39*(12), 1321–1342. https://doi.org/10.1002/eqe.995

Bradley, B. (2011). Empirical equations for the prediction of displacement spectrum intensity and its correlation with other intensity measures. *Soil Dynamics and Earthquake Engineering*, *31*(8), 1182–1191. https://doi.org/10.1016/j.soildyn.2011.04.007

Bradley, B. (2015). Correlation of Arias intensity with amplitude, duration and cumulative intensity measures. *Soil Dynamics and Earthquake Engineering*, *78*, 89–98. https://doi.org/10.1016/j.soildyn.2015.07.009

Buratti, N. (2012). A comparison of the performances of various ground-motion intensity measures. In *15th World Conference on Earthquake Engineering*. https://www.iitk.ac.in/nicee/wcee/article/WCEE2012_5499.pdf

Chandramohan, R., Baker, J. W., & Deierlein, G. G. (2016). Quantifying the influence of ground motion duration on structural collapse capacity using spectrally equivalent records. *Earthquake Spectra*, *32*(2), 927–950. https://doi.org/10.1193/122813eqs298mr2

Cheng, Y., Lucchini, A., & Mollaioli, F. (2015). Correlation of elastic input energy equivalent velocity spectral values. *Earthquakes and Structures*, *8*(5), 957–976. https://doi.org/10.12989/eas.2015.8.5.957

Chopra, A. K. (2006). Elastic response spectrum: a historical note. *Earthquake Engineering & Structural Dynamics*, *36*(1), 3–12. https://doi.org/10.1002/eqe.609

Chou, C., & Uang, C. (2000). Establishing absorbed energy spectra?an attenuation approach. *Earthquake Engineering & Structural Dynamics*, *29*(10), 1441–1455. https://doi.org/10.1002/1096-9845(200010)29:10

Code_Aster - Opensource finite element software. (n.d.). [Software]. https://code-aster.org/V2/spip.php?rubrique2

Cordova, P., Deierlein, G. G., Mehanny, S. S. F., & Cornell, C. A. (2001). Development of a two-parameter seismic intensity measure and probabilistic assessment procedure. *Journal of Engineering and Applied Science*, *51*(2). https://www.researchgate.net/profile/Gregory_Deierlein/publication/228763557_Development_of_a_two-parameter_seismic_intensity_measure_and_probabilistic_assessment_procedure/links/0c96052efb77425a47000000.pdf

Cornell, C. A., & Krawinkler, H. (2000). Progress and challenges in seismic performance assessment. *PEER Cent News*, *3*(2). https://apps.peer.berkeley.edu/news/2000spring/performance.html

Cornell, C. A., & Shome, N. (1999). *Probabilistic seismic demand analysis of nonlinear structures*. https://dl.acm.org/citation.cfm?id=928965

Dávalos, H., & Miranda, E. (2019). Filtered incremental velocity: A novel approach in intensity measures for seismic collapse estimation. *Earthquake Engineering & Structural Dynamics*, *48*(12), 1384–1405. https://doi.org/10.1002/eqe.3205

Decanini, L. D., & Mollaioli, F. (1998). Formulation of elastic earthquake input energy spectra. *Earthquake Engineering & Structural Dynamics*, *27*(12), 1503–1522. https://doi.org/10.1002/(sici)1096-9845(199812)27:12

Decanini, L. D., & Mollaioli, F. (2001). An energy-based methodology for the assessment of seismic demand. *Soil Dynamics and Earthquake Engineering*, *21*(2), 113–137. https://doi.org/10.1016/s0267-7261(00)00102-0

De Biasio, M., Grange, S., Dufour, F., Allain, F., & Petre-Lazar, I. (2014). A simple and efficient intensity measure to account for nonlinear structural behavior. *Earthquake Spectra*, *30*(4), 1403–1426. https://doi.org/10.1193/010614eqs006m

DOI Name 10.1061 values. (n.d.). https://doi.org/10.1061

Dolšek, M. (2008). Incremental dynamic analysis with consideration of modeling uncertainties. *Earthquake Engineering & Structural Dynamics*, *38*(6), 805–825. https://doi.org/10.1002/eqe.869

Eads, L., Miranda, E., & Lignos, D. G. (2015). Average spectral acceleration as an intensity measure for collapse risk assessment. *Earthquake Engineering & Structural Dynamics*, *44*(12), 2057–2073. https://doi.org/10.1002/eqe.2575

Ebrahimian, H., Jalayer, F., Lucchini, A., Mollaioli, F., & Manfredi, G. (2015). Preliminary ranking of alternative scalar and vector intensity measures of ground shaking. *Bulletin of Earthquake Engineering*, *13*(10), 2805–2840. https://doi.org/10.1007/s10518-015-9755-9

Elefante, L., Jalayer, Iervolino, I., & Manfredi, G. (2011). Efficient Seismic Risk Analysis: Disaggregation-based Weighting of Non-linear Dynamic Analysis Results. *14th ECEE*. http://wpage.unina.it/iuniervo/papers/995.pdf

Elhout, E. (2020). The correlation between the ground motion intensity measure parameters of earthquakes. *Asian Journal of Civil Engineering*, *21*(5), 829–840. https://doi.org/10.1007/s42107-020-00243-1

Ellingwood, B. R., & Kinali, K. (2009). Quantifying and communicating uncertainty in seismic risk assessment. *Structural Safety*, *31*(2), 179–187. https://doi.org/10.1016/j.strusafe.2008.06.001

EPRI. (1988). *A criterion for determining exceedance of the operating basis earthquake* (No. 5930). Electric Power Research Institute EPRI, Palo Alto, CA.

EPRI. (1991). *Generic Seismic Ruggedness of Power Plant Equipment (Revision 1)* (Technical Report). Electric Power Research Institute EPRI, Palo Alto, CA.

EPRI. (2003). *Seismic Probabilistic Risk Assessment Implementation* (Report 1002989). Electric Power Research Institute EPRI, Palo Alto, CA.

EPRI. (2007). *Program on Technology Innovation: Validation of CLASSI and SASSI codes to treat Seismic Wave Incoherence in Soil-Structure Interaction (SSI) analysis of nuclear power plant structures* (No. 1015111). Electric Power Research Institute EPRI, Palo Alto, CA.

EPRI. (2018). *Program on Technology Innovation: Seismic Fragility and Seismic Margin Guidance for Seismic Probabilistic Risk Assessments* (No. 3002012994). Electric Power Research Institute EPRI, Palo Alto, CA.

Fajfar, P., Vidic, T., & Fischinger, M. (1990). A measure of earthquake motion capacity to damage medium-period structures. *Soil Dynamics and Earthquake Engineering*, *9*(5), 236–242. https://doi.org/10.1016/s0267-7261(05)80002-8

Gehl, P., Douglas, J., & Seyedi, D. (2015). Influence of the number of dynamic analyses on the accuracy of structural response estimates. *Earthquake Spectra*, *31*(1), 97–113. https://doi.org/10.1193/102912eqs320m

Giovenale, P., Cornell, C. A., & Esteva, L. (2004). Comparing the adequacy of alternative ground motion intensity measures for the estimation of structural responses. *Earthquake Engineering & Structural Dynamics*, *33*(8), 951–979. https://doi.org/10.1002/eqe.386

Hariri-Ardebili, M. A., & Saouma, V. E. (2016). Probabilistic seismic demand model and optimal intensity measure for concrete dams. *Structural Safety*, *59*, 67–85. https://doi.org/10.1016/j.strusafe.2015.12.001

Heshmati, M., & Jahangiri, V. (2021). Appropriate intensity measures for probabilistic seismic demand estimation of steel diagrid systems. *Engineering Structures*, *249*, 113260. https://doi.org/10.1016/j.engstruct.2021.113260

Housner, G. W. (1952). Spectrum intensities of Strong-Motion earthquakes. In *Earthquake Engineering Research Institute eBooks* (pp. 20–36). https://ci.nii.ac.jp/naid/10007257505

Huang, Y., Whittaker, A. S., & Luco, N. (2011). A probabilistic seismic risk assessment procedure for nuclear power plants: (I) Methodology. *Nuclear Engineering and Design*, *241*(9), 3996–4003. https://doi.org/10.1016/j.nucengdes.2011.06.051

Jalayer, F. (2003). *Direct probabilistic seismic analysis: implementing non-linear dynamic assessments* [PhD]. Thesis, Department of Civil and Environmental Engineering, Stanford University, Stanford, CA.

Jalayer, F., Beck, J. L., & Zareian, F. (2012). Analyzing the sufficiency of alternative scalar and vector intensity measures of ground shaking based on information theory. *Journal of Engineering Mechanics-asce*, *138*(3), 307–316. https://doi.org/10.1061/(asce)em.1943-7889.0000327

Jalayer, F., Franchin, P., & Pinto, P. E. (2007). A scalar damage measure for seismic reliability analysis of RC frames. *Earthquake Engineering & Structural Dynamics*, *36*(13), 2059–2079. https://doi.org/10.1002/eqe.704

Jayaram, N., Lin, T., & Baker, J. W. (2011). A computationally efficient Ground-Motion selection algorithm for matching a target response spectrum mean and variance. *Earthquake Spectra*, *27*(3), 797–815. https://doi.org/10.1193/1.3608002

Kappos, A. (1990). Sensitivity of calculated inelastic seismic response to input motion characteristics. *Proceedings of the 4th National Conference on Earthquake Engineering, Palm Springs, CA, USA, 20-24 May 1990*, *2*, 25–34.

Kazantzi, A. K., & Vamvatsikos, D. (2015). Intensity measure selection for vulnerability studies of building classes. *Earthquake Engineering & Structural Dynamics*, *44*(15), 2677–2694. https://doi.org/10.1002/eqe.2603

Kennedy, R., Cornell, C. A., Campbell, R. D., Kaplan, S., & Perla, H. (1980). Probabilistic seismic safety study of an existing nuclear power plant. *Nuclear Engineering and Design*, *59*(2), 315–338. https://doi.org/10.1016/0029-5493(80)90203-4

Kennedy, R., & Ravindra, M. (1984). Seismic fragilities for nuclear power plant risk studies. *Nuclear Engineering and Design*, *79*(1), 47–68. https://doi.org/10.1016/0029-5493(84)90188-2

Kim, C., Jeong, E. H., & Shin, M. (2021). Seismic performance assessment of NPP concrete containments considering recent ground motions in South Korea. *Nuclear Engineering and Technology*. https://doi.org/10.1016/j.net.2021.07.035

Kohrangi, M., Bakalis, K., Triantafyllou, G., Vamvatsikos, D., & Bazzurro, P. (2023). Hazard consistent record selection procedures accounting for horizontal and vertical components of the ground motion: Application to liquid storage tanks. *Earthquake Engineering & Structural Dynamics*, *52*(4), 1232–1251. https://doi.org/10.1002/eqe.3813

Kohrangi, M., Bazzurro, P., & Vamvatsikos, D. (2016). Vector and Scalar IMs in Structural Response Estimation, Part I: Hazard Analysis. *Earthquake Spectra*, *32*(3), 1507–1524. https://doi.org/10.1193/053115eqs080m

Kotha, S. R., Weatherill, G., Bindi, D., & Cotton, F. (2020). A regionally-adaptable ground-motion model for shallow crustal earthquakes in Europe. *Bulletin of Earthquake Engineering*, *18*(9), 4091–4125. https://doi.org/10.1007/s10518-020-00869-1

Kramer, S. L. (1993). *Geotechnical earthquake engineering*. rentice-Hall Civil Engineering and Engineering Mechanics Series, Prentice Hall, Upper Saddle River.

Kramer, S. L. (2013). Performance-based design methodologies for geotechnical earthquake engineering. *Bulletin of Earthquake Engineering*, *12*(3), 1049–1070. https://doi.org/10.1007/s10518-013-9484-x

Lanzano, G., Felicetta, C., Pacor, F., Spallarossa, D., & Traversa, P. (2022). Generic-To-Reference rock scaling factors for seismic ground motion in Italy. *Bulletin of the Seismological Society of America*, *112*(3), 1583–1606. https://doi.org/10.1785/0120210063

Li, B., & Cai, Z. (2022). Effectiveness of vector intensity measures in probabilistic seismic demand assessment. *Soil Dynamics and Earthquake Engineering*, *155*, 107201. https://doi.org/10.1016/j.soildyn.2022.107201

Liel, A. B., Haselton, C. B., Deierlein, G. G., & Baker, J. W. (2009). Incorporating modeling uncertainties in the assessment of seismic collapse risk of buildings. *Structural Safety*, *31*(2), 197–211. https://doi.org/10.1016/j.strusafe.2008.06.002

Lin, T., Haselton, C. B., & Baker, J. W. (2013). Conditional spectrum-based ground motion selection. Part I: Hazard consistency for risk-based assessments. *Earthquake Engineering & Structural Dynamics*, *42*(12), 1847–1865. https://doi.org/10.1002/eqe.2301

Luco, N., & Cornell, C. A. (2007). Structure-Specific scalar intensity measures for Near-Source and ordinary earthquake ground motions. *Earthquake Spectra*, *23*(2), 357–392. https://doi.org/10.1193/1.2723158

Mackie, K. R., & Stojadinović, B. (2001). Probabilistic Seismic demand model for California Highway bridges. *Journal of Bridge Engineering*, *6*(6), 468–481. https://doi.org/10.1061/(asce)1084-0702(2001)6:6(468

Marafi, N. A., Berman, J. W., & Eberhard, M. O. (2015). Ductility-dependent intensity measure that accounts for ground-motion spectral shape and duration. *Earthquake Engineering & Structural Dynamics*, *45*(4), 653–672. https://doi.org/10.1002/eqe.2678

Martinez-Rueda, J. (1998). Scaling procedure for natural accelerograms based on a system of spectrum intensity scales. *Earthquake Spectra*, *14*(1), 135–152. https://doi.org/10.1193/1.1585992

Matsumura, K. (1991). On the intensity measure of strong motion related to structural failures. *Proceedings of the 10th World Conference on Earthquake Engineering, Rotterdam, the Netherlands, 19–24 July 1992*, 375–380. https://www.iitk.ac.in/nicee/wcee/article/10_vol1_375.pdf

Moehle, J. P., & Deierlein, G. G. (2004). A framework methodology for performance-based earthquake engineering. *Proceedings of the 13th World Conference on Earthquake Engineering, Vancouver, Canada, 1–6 August*.

Mollaioli, F., Lucchini, A., Cheng, Y., & Monti, G. (2013). Intensity measures for the seismic response prediction of base-isolated buildings. *Bulletin of Earthquake Engineering*, *11*(5), 1841–1866. https://doi.org/10.1007/s10518-013-9431-x

Nguyen, D., Thusa, B., Azad, S., Tran, V., & Lee, T. H. (2021). Optimal earthquake intensity measures for probabilistic seismic demand models of ARP1400 reactor containment building. *Nuclear Engineering and Technology*, *53*(12), 4179–4188. https://doi.org/10.1016/j.net.2021.06.034

Nguyen, D., Thusa, B., Han, T. S., & Lee, T. H. (2020). Identifying significant earthquake intensity measures for evaluating seismic damage and fragility of nuclear power plant structures. *Nuclear Engineering and Technology*, *52*(1), 192–205. https://doi.org/10.1016/j.net.2019.06.013

Nicknam, A., Eftekhari, N., Mazarei, A., & Ganjvar, M. (2015). A three elements vector valued structure's ultimate Strength-Strong Motion-Intensity measure. *International Journal of Civil and Environmental Engineering*, *9*(11). https://www.researchgate.net/publication/305318820_A_Three_Elements_Vector_Valued_Structure's_Ultimate_Strength-Strong_Motion-Intensity_Measure

Noh, H. Y., Lallemant, D., & Kiremidjian, A. S. (2014). Development of empirical and analytical fragility functions using kernel smoothing methods. *Earthquake Engineering & Structural Dynamics*, *44*(8), 1163–1180. https://doi.org/10.1002/eqe.2505

Nuttli, O. W. (1979). State-of-the-art for assessing earthquake hazards in the United States. Report 16, The relation of sustained maximum ground acceleration and velocity to earthquake intensity and magnitude. *This Digital Resource Was Created From Scans of the Print Resource*. https://erdc-library.erdc.dren.mil/jspui/bitstream/11681/20749/1/MP-S-73-1-Report-16.pdf

Pacific Earthquake Engineering Research Center, University of California, Berkeley. (2006). *OpenSees*. Open System for Earthquake Engineering Simulation. http://opensees.berkeley.edu/

Padgett, J. E., Nielson, B. G., & DesRoches, R. (2008). Selection of optimal intensity measures in probabilistic seismic demand models of highway bridge portfolios. *Earthquake Engineering & Structural Dynamics*, *37*(5), 711–725. https://doi.org/10.1002/eqe.782

Pagani, M., Chartier, T., & Rood, A. (2023). *Application to METIS Study Case (WP4) METIS Deliverable D4.6*. https://metis-h2020.eu/wp-content/uploads/2023/05/METIS_D4_6_Application_to_METIS_study_case_submitted_20_03_2023_V1.pdf

Pagani, M., Monelli, D., Weatherill, G., Danciu, L., Crowley, H., Silva, V., Henshaw, P., Butler, L., Nastasi, M., Panzeri, L., Simionato, M., & Viganò, D. (2014). OpenQuake Engine: an open hazard (and risk) software for the global earthquake model. *Seismological Research Letters*, *85*(3), 692–702. https://doi.org/10.1785/0220130087

Park, Y., Ang, A. H., & Wen, Y. K. (1985). Seismic damage analysis of reinforced concrete buildings. *Journal of Structural Engineering-asce*, *111*(4), 740–757. https://doi.org/10.1061/(asce)0733-9445(1985)111:4(740

Porter, K., Kennedy, R., & Bachman, R. E. (2007). Creating fragility functions for Performance-Based Earthquake Engineering. *Earthquake Spectra*, *23*(2), 471–489. https://doi.org/10.1193/1.2720892

Rajeev, P., Franchin, P., & Pinto, P. E. (2008). Increased accuracy of Vector-IM-Based seismic risk assessment? *Journal of Earthquake Engineering*, *12*(sup1), 111–124. https://doi.org/10.1080/13632460801925798

Rathje, E. M., Abrahamson, N. A., & Bray, J. D. (1998). Simplified Frequency Content Estimates of Earthquake Ground Motions. *Journal of Geotechnical and Geoenvironmental Engineering*. https://doi.org/10.1061/(ASCE)1090-0241(1998)124:2(150

Rezaeemanesh, M., & Mashayekhi, M. (2022). Investigating the Correlation between the Parameters of Ground Motion Intensity Measures for Iran's Data. *Journal of Soft Computing in Civil Engineering*, *6*(4).

Riddell, R., & García, J. E. (2001). Hysteretic energy spectrum and damage control. *Earthquake Engineering & Structural Dynamics*, *30*(12), 1791–1816. https://doi.org/10.1002/eqe.93

Rossetto, T., Ιωάννου, I., Grant, D., & Maqsood, T. (2014). Guidelines for the empirical vulnerability assessment. *GEM Technical Report 2014–08 V1.0.0. GEM Foundation, Pavia, Italy.* https://doi.org/10.13117/GEM.VULN-MOD.TR2014.11

Ryan, K. L., Soroushian, S., Maragakis, E. M., Sato, E., Sasaki, T., & Okazaki, T. (2016). Seismic simulation of an integrated Ceiling-Partition Wall-Piping system at E-Defense. i: Three-Dimensional structural response and base isolation. *Journal of Structural Engineering-asce*, *142*(2). https://doi.org/10.1061/(asce)st.1943-541x.0001384

Sainct, R., Feau, C., Martinez, J., & Garnier, J. (2020). Efficient methodology for seismic fragility curves estimation by active learning on Support Vector Machines. *Structural Safety*, *86*, 101972. https://doi.org/10.1016/j.strusafe.2020.101972

Salome-Meca platform. (n.d.). [Software]. https://code-aster.org/V2/spip.php?article303

Scott, M., & Fillipou, F. (2014). *Hysteretic material - OpenSeesWiki*. https://opensees.berkeley.edu/wiki/index.php/Hysteretic_Material

SEAOC. (1995). *Vision 2000*. https://www.hsdl.org/?view&did=788527

Shome, N., & Cornell, C. A. (1999). *Probabilistic seismic demand analysis of nonlinear structures*. RMS Program, Stanford University, Report No. RMS35.

Shome, N., Cornell, C. A., Bazzuro, P., & Carballo, J. E. (1998). Earthquakes, records, and nonlinear responses. *Earthq Spectra*, *14*(3), 469–500.

Šipčić, N., García De Quevedo Iñarritu, P., & Kohrangi Mohsen. (2023). *Methodology for selecting ensembles of hazard-consistent ground motions suitable for fragility curve computations for clustered seismicity and datasets for WP6. METIS Deliverable D5.2.* https://metis-h2020.eu/wp-content/uploads/2023/06/D5_2_Methodology_for_selecting_ensembles_of_rock_hazard_consistent_ground_motions_suitable_br___for_fragility_curves_computations_for_clustered_seismicity_and_dataset_V2.pdf

Soroushian, S., Maragakis, E. M., Ryan, K. L., Sato, E., Sasaki, T., Okazaki, T., & Mosqueda, G. (2016). Seismic simulation of an integrated Ceiling-Partition Wall-Piping system at E-Defense. II: Evaluation of nonstructural damage and fragilities. *Journal of Structural Engineering-asce*, *142*(2). https://doi.org/10.1061/(asce)st.1943-541x.0001385

Spillatura, A., Kohrangi, M., Bazzurro, P., & Vamvatsikos, D. (2021). Conditional spectrum record selection faithful to causative earthquake parameter distributions. *Earthquake Engineering & Structural Dynamics*, *50*(10), 2653–2671. https://doi.org/10.1002/eqe.3465

Tavakoli, B., & Pezeshk, S. (n.d.). Selection of optimal ground motion parameters for nonlinear dynamic analysis of structures. *Journal of Earthquake Engineering*, *9(2)*, 283–310.

Thun, J., Roehm, L. H., Scott, G. A., & Wilson, J. A. (1988). Earthquake ground motions for design and analysis of dams. *Geotechnical Special Publication*, *20*, 463–481. https://cedb.asce.org/CEDBsearch/record.jsp?dockey=0056815

Trevlopoulos, K., & Zentner, I. (2019). Seismic Fragility Curve Assessment Based on Synthetic Ground Motions with Conditional Spectra. *Pure and Applied Geophysics*, *177*(5), 2375–2390. https://doi.org/10.1007/s00024-019-02245-w

Uang, C., & Bertero, V. V. (1990). Evaluation of seismic energy in structures. *Earthquake Engineering & Structural Dynamics*, *19*(1), 77–90. https://doi.org/10.1002/eqe.4290190108

Vamvatsikos, D. (2014). Seismic Performance Uncertainty Estimation via IDA with Progressive Accelerogram-Wise Latin Hypercube Sampling. *Journal of Structural Engineering-asce*, *140*(8). https://doi.org/10.1061/(asce)st.1943-541x.0001030

Vamvatsikos, D., & Cornell, C. A. (2001). Incremental dynamic analysis. *Earthquake Engineering & Structural Dynamics*, *31*(3), 491–514. https://doi.org/10.1002/eqe.141

Vamvatsikos, D., & Cornell, C. A. (2005). Developing efficient scalar and vector intensity measures for IDA capacity estimation by incorporating elastic spectral shape information. *Earthquake Engineering and Structural Dynamics/Earthquake Engineering & Structural Dynamics*, *34*(13), 1573–1600. https://doi.org/10.1002/eqe.496

Vamvatsikos, D., & Fragiadakis, M. (2009). Incremental dynamic analysis for estimating seismic performance sensitivity and uncertainty. *Earthquake Engineering & Structural Dynamics*, *39*(2), 141–163. https://doi.org/10.1002/eqe.935

Weatherill, G., Kotha, S. R., & Cotton, F. (2020). A regionally-adaptable "scaled backbone" ground motion logic tree for shallow seismicity in Europe: application to the 2020 European seismic hazard model. *Bulletin of Earthquake Engineering*, *18*(11), 5087–5117. https://doi.org/10.1007/s10518-020-00899-9

Whittaker, A., Deierlein, G. G., Hooper, J., & Merovich, A. (2004). Engineering demand parameters for structural framing systems. *ResearchGate*. https://doi.org/10.13140/RG.2.1.4207.8321

Willaume, P., & Noret, E. (2011). Présentation du modèle brochette. In *EDF* (DT-PMPE-00234-002-B).

Wolf, J. P. (1998). Simple physical models for foundation dynamics. In *Developments in Geotechnical Engineering* (pp. 1–70). https://doi.org/10.1016/s0165-1250(98)80004-7

Yakhchalian, M., Nicknam, A., & Amiri, G. G. (2015). Optimal vector-valued intensity measure for seismic collapse assessment of structures. *Earthquake Engineering and Engineering Vibration*, *14*(1), 37–54. https://doi.org/10.1007/s11803-015-0005-6

Yang, C., Xie, L., Li, A., Jia, J., & Zeng, D. (2019). Ground motion intensity measures for seismically isolated RC tall buildings. *Soil Dynamics and Earthquake Engineering*, *125*, 105727. https://doi.org/10.1016/j.soildyn.2019.105727

Zavala, N., Bojórquez, E., Barraza, M., Bojórquez, E., Villela, A., Campos-Gaytán, J. R., Torres, J. I., Sánchez, R., & Carvajal, J. (2023). Vector-Valued intensity measures based on spectral shape to predict seismic fragility surfaces in reinforced concrete buildings. *Buildings*, *13*(1), 137. https://doi.org/10.3390/buildings13010137

Zelaschi, C., Monteiro, R., & Pinho, R. (2017). Critical assessment of intensity measures for seismic response of Italian RC Bridge portfolios. *Journal of Earthquake Engineering*, *23*(6), 980–1000. https://doi.org/10.1080/13632469.2017.1342293

Zentner, I. (2017). A general framework for the estimation of analytical fragility functions based on multivariate probability distributions. *Structural Safety*, *64*, 54–61. https://doi.org/10.1016/j.strusafe.2016.09.003

Zentner, I., Gündel, M., & Bonfils, N. (2017). Fragility analysis methods: Review of existing approaches and application. *Nuclear Engineering and Design*, *323*, 245–258. https://doi.org/10.1016/j.nucengdes.2016.12.021

Zentner, I., Humbert, N., Ravet, S., & Viallet, E. (2011). Numerical methods for seismic fragility analysis of structures and components in nuclear industry - Application to a reactor coolant system. *Georisk: Assessment and Management of Risk for Engineered Systems and Geohazards*, *5*(2), 99–109. https://doi.org/10.1080/17499511003630512

Zhang, Y., He, Z., & Yang, Y. (2017). A spectral-velocity-based combination-type earthquake intensity measure for super high-rise buildings. *Bulletin of Earthquake Engineering*, *16*(2), 643–677. https://doi.org/10.1007/s10518-017-0224-5

Zhou, Y., Ge, P., Han, J., & Lu, Z. (2017). Vector-valued intensity measures for incremental dynamic analysis. *Soil Dynamics and Earthquake Engineering*, *100*, 380–388. https://doi.org/10.1016/j.soildyn.2017.06.014